Degradation of Groundwater Contaminants by Iron Containing Systems

A THESIS
SUBMITTED TO THE FACULTY OF THE GRADUATE SCHOOL
OF THE UNIVERSITY OF MINNESOTA
BY

Kirsten Marie Moore

IN PARTIAL FULFILLMENT OF THE REQUIREMENTS
FOR THE DEGREE OF
MASTER OF SCIENCE

Dr. William A. Arnold, Advisor
Dr. R. Lee Penn, Co-Advisor

September 2010

Acknowledgements

I would like to first thank my advisor Dr. Bill Arnold and co-advisor Dr. Lee Penn. My graduate work would not have been possible without their guidance and support. I would also like to thank the Arnold and Penn group members for their help and friendship during my time in graduate school. In particular I would like to thank Jason Myers and Erin Surdo for their guidance in the lab. I would also like to thank my family. My mom and husband Ross have provided unwavering patience, support, and love during my academic career and my success would not be possible without them.

Abstract

Iron-containing systems are effective at reducing common groundwater contaminants. Zero-valent iron particles are an effective remediation technology for groundwater contaminated with halogenated organic compounds. Iron salts were used to generate iron oxide nanoparticles, which were reduced to zero-valent iron. The reactivity of the resulting zero-valent iron nanoparticles was quantified by monitoring the kinetics of carbon tetrachloride reduction, and significant differences in reactivity were observed. Furthermore, substantial variations in the solid-state products of oxidation were also observed.

Fe(II)-iron mineral systems are also an effective method for reducing nitroaromatic compounds, such as pesticides. The objective of this study was to link changes in the mineralogy of goethite particles to changes in the reactivity of an Fe(II)-goethite system. The reactivity of Fe(II)-goethite and Fe(II)-goethite sand systems were quantified by monitoring the kinetics of trifluralin reduction. Changes in the goethite mineralogy were observed by transmission electron microscopy. Differences in goethite reactivity and the solid-state products were observed, as compared to previous work using goethite.

Table of Contents

List of Tables

List of Figures

Chapter 1: Introduction

1.1 Groundwater Contaminants

Groundwater is an important resource that is used for drinking water, irrigation, public supply, and numerous industries. In 2000, the U.S. Geological Survey estimated that 21% of all water used in the U.S. came from groundwater, with the remaining supply from surface water *(1)*. People who do not have access to a public water supply obtain 98% of their water from groundwater *(1)*. As a result of the importance of groundwater, contamination of this resource is a concern. Contaminants can enter groundwater as a result of seepage from landfills and disposal sites, spills or leaks, and application of pesticides and herbicides *(2-4)*. Common groundwater contaminants include metals, volatile organic compounds, and pesticides *(3, 4)*.

Chlorinated solvents are among the most common organic groundwater contaminants *(2, 3, 5)*. Chlorinated solvents are used in a variety of commercial and industrial products such as degreasing of airplane and automobile parts, dry cleaning, and fumigation. Due to their widespread use, chlorinated solvents are frequently found in groundwater and account for 9 of the top 20 contaminants found in groundwater at Superfund sites *(2)*. Some of the most common chlorinated solvents found in groundwater include trichloroethene (TCE), tetrachloroethene (PCE), carbon tetrachloride (CT), and 1,1,1-trichloroethane (TCA) *(5)*. These compounds penetrate groundwater in the form of a dense non-aqueous phase liquid (DNAPL) and from there sorb to soil or dissolve in groundwater, where they can continue to migrate under the influence of the hydraulic gradient *(5)*. Chlorinated solvents can also volatilize and be

present as a vapor in soils and the vadose zone. These compounds tend to be difficult to remediate due their low solubility in water and resistance to degradation and are thus persistent in the environment.

Pesticides are another class of compounds commonly detected in groundwater. They are used to control pests such as weeds and insects on cropland. Pesticides are applied directly to soil or to the plants, depending on the pesticide. After application they can reach groundwater by several pathways, including runoff from fields and leaching through soil *(6)*. Pesticide use in the U.S. was estimated to be five billion pounds by the U.S EPA during 2000 and 2001 *(7)*. As a result of such high usage and their resistance to degradation, many pesticides have been detected in groundwater throughout the U.S. A ten year study performed between 1992 and 2001 by the USGS sampled various streams and groundwater supplies throughout the U.S. The study determined that over half of the sampled shallow groundwater supplies contained one or more pesticides, and a third of the deep water wells and aquifers contained one or more pesticides and/or pesticide degradates *(8)*. Pesticides were found in both agricultural and urban areas, though pesticide levels were usually higher in agricultural areas. Most of the pesticide concentrations were below human health standards. Some of the most commonly detected and used herbicides include atrazine, metolachlor, alachlor, acetochlor, simazine, 2,4-D, prometon, glyphosate, pendimethalin, and trifluralin *(7, 8)*.

Concerns have been raised over the presence of pesticides in groundwater due to their potential negative impacts on human life and the ecosystem. Many pesticides are suspected or known carcinogens. They often affect the nervous system and are eye and

skin irritants for humans *(9)*. Many pesticides are also suspected endocrine disruptors. Pesticides that are known or suspected endocrine distruptors include 2,4-D, alachlor, atrazine, trifluralin, DDT, and methoxychlor *(10)*. Numerous other pesticides have also been implicated *(10-12)*.

1.2 Groundwater Remediation Techniques

Due to the presence and persistence of numerous groundwater contaminants, various remediation technologies have been developed. Remediation technologies include both *in situ* and *ex situ* techniques. *In situ* remediation techniques include bioremediation, soil vapor extraction, permeable reactive barriers (PRBs), and chemical oxidation or reduction *(13)*. *Ex situ* techniques include bioreactors, carbon absorption, ion exchange, and membrane separation *(13)*. An advantage of *in situ* remediation is that the contaminated water or soil does not have to be pumped (water) or excavated (soil).

Chlorinated solvents can undergo biodegradation and chemical transformation. All of the mentioned *in situ* remediation technologies, therefore, can be used to remove these compounds. Chemicals such as TCE and TCA are aerobically degraded by cometabolism if appropriate bacteria are present *(2, 14)*. Chlorinated compounds can also undergo anaerobic biodegradation by reductive dehalogenation *(2, 14)*. These compounds are also degraded via chemical reduction techniques using PRBs and *in situ* redox manipulation. One option for chemical reduction is using zero-valent metals, such as iron, which can be incorporated into PRBs or used separately. Pesticides can be removed using *ex situ* techniques by pumping contaminated water through carbon filters

(15). Chemical and biological oxidation processes can also be used to remediate pesticides *in situ (16)*.

1.3 Zero-Valent Iron for Remediation of Chlorinated Groundwater Contaminants

Zero-valent iron (ZVI) is now a widely used treatment method for reducing chlorinated compounds. Iron is a reducing agent, where oxidation, or corrosion, of ZVI can be described by equation 1-1. Reductive dehalogenation of alkyl halides, RX, in the presence of a proton donor, such as water, is described by equation 1-2 *(17)*.

$$Fe^{2+} + 2e^- \rightarrow Fe^0 \qquad (1\text{-}1)$$

$$RX + 2e^- + H^+ \rightarrow RH + X^- \qquad (1\text{-}2)$$

Combination of reactions 1 and 2 results in conditions that are thermodynamically favorable for reduction of halogenated compounds and corrosion of ZVI *(17)*.

$$Fe^0 + RX + H^+ \rightarrow Fe^{2+} + RH + X^- \qquad (1\text{-}3)$$

Iron is also oxidized by dissolved oxygen or by water itself. Iron corrosion results in the formation of iron oxides on the surface of iron particles. Tthe oxide layer formed over ZVI particles is typically magnetite, Fe_3O_4. Further oxidation of the oxide surface layer occurs via the oxidation of Fe^{II} to Fe^{III}, creating a layer of maghemite (γ-Fe_2O_3) or goethite (FeOOH) *(18)*.

The mechanism by which degradation of halogenated contaminants occurs is reductive dehalogenation *(17)*. Reductive dehalogenation mediated by ZVI is a surface mediated reaction, where electrons must be transferred from the metal particle to the contaminant for dechlorination to occur *(17, 19)*. The main pathways by which this

occurs for chlorinated ethanes and ethenes are hydrogenolysis (equation 1-4), reductive β-elimination (equation 1-5), and catalytic hydrogenolysis by hydrogen gas (equation 1-6), which requires a catalyst *(17, 20-24)*.

$$RH_2Cl\text{-}RH_2Cl + H^+ + 2e^- \leftrightarrow RH_3\text{-}RH_2Cl + Cl^- \quad (1\text{-}4)$$

$$RH_2Cl\text{-}RH_2Cl + 2e^- \leftrightarrow RH_2{=}RH_2 + 2Cl^- \quad (1\text{-}5)$$

$$RH_2Cl\text{-}RH_2Cl + H_2(g) \rightarrow RH_3\text{-}RHCl + H^+ + Cl^- \quad (1\text{-}6)$$

To achieve complete reduction of chlorinated compounds sequential dehalogenation is required. For example, CT is reduced to chloroform, which is further degraded to dichloromethane via hydrogenolysis. In theory, CT can be fully dechlorinated by hydrogenolysis. Further dehalogenation of dichloromethane, however, is very slow in comparison to the first dehalogenation of CT. Due to the persistence of CF and dichloromethane dehalogenation of these compounds does not usually occur in the environment *(25)*. Complete dechlorination of CT, however, is thought to occur by an α-elimination reaction via a dichlorocarbene intermediate. This intermediate undergoes further reduction to methane or hydrolysis to produce formate *(26)*. This process is shown in Figure 1-1.

Ideally, complete dechlorination of chlorinated solvents is highly desirable because the partially dechlorinated compounds, such as chloroform, are also toxic *(27, 28)*. Partially dehlogenated intermediates produced from reduction of TCE and PCE, such as *cis*-1,2-dichloroethene (*cis*-DCE) and vinyl chloride, are also toxic (and in the case of vinyl chloride, of greater concern than the parent compounds) *(29, 30)*.

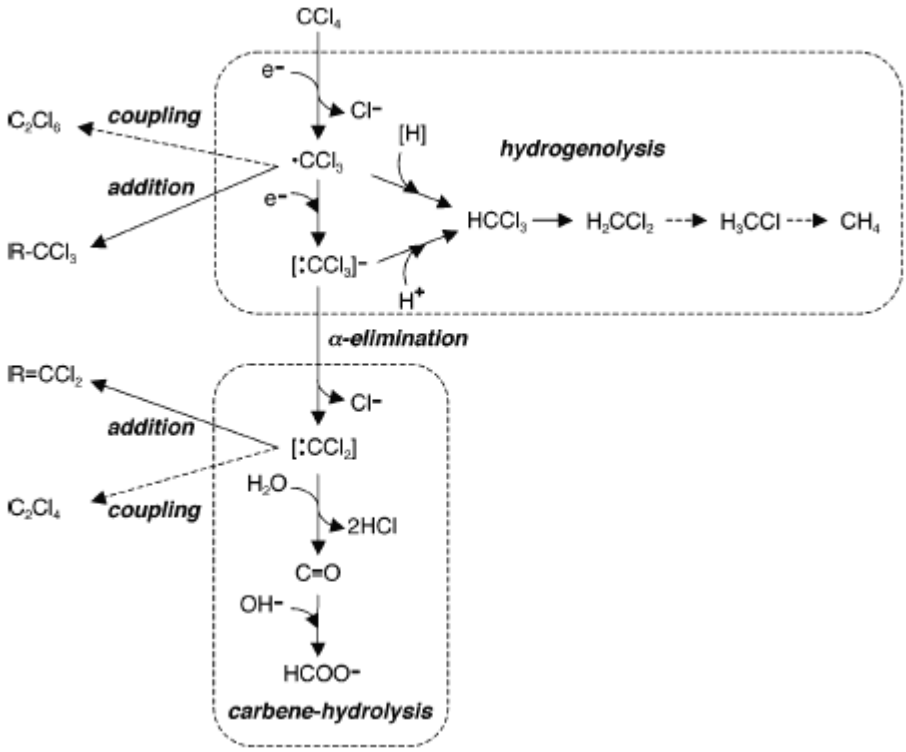

Figure 1-1. CT degradation pathways in an anoxic environment from *(26)*.

ZVI reactions with chlorinated compounds are often described by pseudo-first order kinetics for a given set of conditions (i.e. iron loading, pH, initial contaminant concentration). Equation 1-7 is a simple first order model used to describe the kinetics of CT reduction. Equations 1-8 and 1-9 describe the kinetics of formation and subsequent reduction of the products formed by CT degradation *(17)*:

$$[CT]_t = [CT]_{max} e^{-k_1 t} \quad (1\text{-}7)$$

$$[CF]_t = \frac{[CF]_{max} k_1}{k_2 - k_1} \left(e^{-k_1 t} - e^{-k_2 t}\right) \quad (1\text{-}8)$$

$$[MC]_t = [MC]_{max} \left(1 - e^{-k_2 t}\right) \quad (1\text{-}9)$$

where k_1 is the first order rate constant for CT dechlorination to chloroform (CF) and k_2 is the rate constant for CF dechlorination to methylene chloride (MC), or dichloromethane. Degradation rates can be influenced by environmental conditions such as pH. Studies have demonstrated that decreasing pH can lead to increased degradation rates. Iron corrosion, however, results in increases in pH, which can lead to faster formation of iron hydroxide precipitates on the ZVI particle surface and decrease reaction rates *(17, 31)*. In weakly buffered systems, this increase in pH could lead to a decrease in reaction rates.

While ZVI has been used to successfully reduce halogenated pollutants, much effort has been focused on accelerating reaction rates and increasing the range of contaminants that can be treated. One proposed way to achieve these goals is the use of ZVI nanoparticles. Interest in ZVI nanoparticles has grown because nanoparticle iron can degrade chlorinated compounds more quickly than granular iron. Increasing the available particle surface area may increase ZVI degradation rates with chlorinated compounds due to an increase in the number of available surface sites for reaction *(17, 32-34)*. ZVI nanoparticles have successfully been used for direct injection into contaminated groundwater sites *(32)*. Finally, bimetallic (nano)particles and (nano)particles containing sulfur have been found to have increased reaction rates with chlorinated compounds *(28, 35-40)*.

1.4 Remediation of Nitroaromatic Pesticides by Iron-Bearing Systems

Nitroaromatic compounds (NACs) represent another class of groundwater contaminants that is degraded by systems containing reduced iron. NACs are used as

herbicides, explosives, and textile dyes *(41)*. Nitroaromatic herbicides commonly applied to soil include pendimethalin, trifluralin, benfluralin, and nitralin. These compounds undergo a variety of biotic and abiotic degradation processes. Loss mechanisms for pesticides include volatilization and photolysis after application, but some of the pesticides can migrate through the soil to groundwater. Under standard environmental conditions NACs are reduced to anilines by ZVI as well as surface bound Fe(II) species in the presence of iron oxides such as goethite and magnetite *(42-44)*. The latter is an important degradation process due to the abundance of iron containing minerals and aqueous Fe(II) present in the environment. Fe(II) has been shown to be present in concentrations up to 1 mM in wetlands *(45)* and in landfill leachate *(46)* .

Ferrous iron has been shown to be a powerful reductant when bound to mineral surfaces, whereas aqueous Fe(II) does little to reduce NACs *(41, 42)*. Iron (III) minerals are also not reductants in the absence of Fe(II). Reduction of NACs occurs through electron transfer from Fe(II) to the compound, reducing the NAC to its aniline counterpart. Figure 1-2 depicts a reaction scheme for NACs.

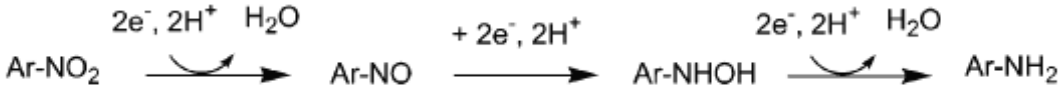

Figure 1-2. Reduction of NACs to their aniline counterparts from *(47)*.

This reaction is thought to occur through the formation of surface complexes of the form =Fe(III)-O-Fe(II)-OH, regardless of the mineral phase *(48)*. Reaction sites on the mineral surfaces can be regenerated by the continued sorption of Fe(II) to the mineral

surface, or by microbial or abiotic reduction of Fe(III) present in the iron(III) (hydr)oxide minerals *(41)*. This allows for continuous degradation of NACs in waters with high $Fe(II)_{aq}$ concentrations or containing iron-reducing bacteria.

Reduction of NACs typically follows pseudo-first order kinetics. Rate constants are dependent on multiple factors, including pH and ionic strength. Reduction of NACs is only significant above pH 6. This is due to the fact that Fe(II) adsorption to iron(III) hydro(oxide) surfaces is pH dependent andsignificantly increases above pH 6 *(42)*. Pseudo-first order rate constants for NACs also increase as pH or Fe(II) concentration increase *(42, 49, 50)*. Increasing ionic strength can also inhibit the reduction of NACs *(49)*.

The effect of various iron minerals on NAC reduction has also been studied. Minerals and materials investigated include iron oxides (magnetite, goethite, lepidocrocite, hematite), iron sulfides (pyrite, sulfate green rust, mackinawite), siderite, montmorillonite clays and FeOOH coated sands *(41, 42, 47, 49)*. These have all successfully reduced NACs in the presence of Fe(II). It is difficult to compare reactivity because many of these studies were performed using different compounds and solution conditions, such as pH and ionic strength. This makes comparison of the studies difficult. Elsner et. al. *(47)* compared the reactivity of iron oxides and iron sulfides under similar reaction conditions using hexachloroethane and 4-chloronitrobenze as probe compounds. Reactions carried out at a near neutral pH indicated that Fe(II) bound to iron sulfides were slightly more reactive than Fe(II) bound to iron oxide. Sulfide is thought to promote electron transfer from Fe(II) or directly transfer electrons to the contaminant

(47). This suggests that the mineral on which reduction of NACs occur plays a role in determining reaction rates *(42, 49)*.

1.5 Scope of Thesis

The purpose of this research is to examine the reactivity of iron-bearing minerals with respect to common groundwater contaminants. ZVI nanoparticles were prepared using ferrihydrite synthesized in the presence of different anions followed by reduction using hydrogen gas at high temperature. The reactivity of the ZVI particles was determined in batch kinetic experiments by quantifying the degradation rate of carbon tetrachloride (Chapter 2). Particles were well characterized before and after reaction. Reductive degradation of the nitroaromatic herbicide trifluralin was also investigated (Chapter 3). Kinetic experiments quantifying the degradation rate of trifluralin were performed using synthetic goethite and goethite containing sand in the presence of aqueous Fe(II). The goethite nanocrystal size, shape, and composition were characterized before and after reaction by transmission electron microscopy and X-ray diffraction to link changes in reactivity during experiments to changes in the particle surface mineralogy.

1.6 References

1. USGS Groundwater use in the United States. http://ga.water.usgs.gov/edu/wugw.html (July, 2010).

2. National Research Council Committee of Innovative Remediation Technologies, ed. *Innovations in Ground Water and Soil Cleanup: From Concept to Commercialization*. 1997, National Academies Press: Washington D.C. 113-120.

3. Barcelona, M. J. *Contamination of Ground water: Prevention, Assessment, Restoration*. 184 ed. Pollution Technology Review. 1990: William Andrew, Incorporated. p. 228.

4. Lee, C. C. and Lin, S. D. *Water and Wastewater Calculations Manual*. 2nd ed. 2007: McGraw-Hill Professional. p. 211-214.

5. EPA. In *Proceedings of the Symposium on Natural Attenuation of Chlorinated Organics*, Dallas, Texas, 1996; EPA, Office of Research and Development, U.S. EPA: Dallas, Texas, 1996; p. 7-11.

6. *In Situ Thermal Treatment of Chlorinated Solvents: Fundamentals and Field Applications*. EPA 542-R-04-010. 2004, Washington, D.C.: U.S. EPA Office of Solid Waste and Emergency Response. p. 7-12.

7. Bicki, T. J. *Pesticides and Groundwater: Pesticides as Potential Pollutants*; University of Illinois at Urbana-Champaign College of Agricultural, Consumer and Environmental Sciences: 1989; p. 3-9.

8. Keily, T.;Donaldson, D. and Grube, A. *Pesticides Industry Sales and Usage: 2000 and 2001 Market Estimates*; U.S. EPA Office of Prevention, Pesticides, and Toxic Substances: Washington, D.C., 2004; p. 16-31.

9. Gilliom, R. J. and Hamilton, P. A. *Pesticides in the Nation's Streams and Ground Water: 1992-2001 A Summary*; USGS: Sacramento, CA, 2006; p. 1-6.

10. Pesticides: Health and Safety: Human Health Issues. http://www.epa.gov/pesticides/health/human.htm (July, 2010).

11. Matthews, G. A. *Pesticides: Health, Safety, and the Environment*. 2006, Ames, IA: Wiley-Blackwell. p. 42-43.

12. Gasnier, C.;Dumont, C.;Benachour, N.;Clair, E.;Chagnon, M.-C. and Seralini, G.-E. *Glyphosate-based herbicides are toxic and endocrine disruptors in human cell lines.* Toxicology. **2009**, *262*(3), p. 184-191.

13. Colborn, T. and Short, P. *Pesticide use in the U.S and policy implications: A focus on herbicides.* Toxicology and Industrial Health. **1999**, *15*, p. 241-276.

14. Delleur, J. W. *The Handbook of Groundwater Engineering, 2nd Edition*. 2006, Boca Raton, FL: CRC Press. p. 36-30 - 36-33.

15. McCarty, P. L. In *Groundwater quality: natural and enhanced restoration of groundwater*, Groundwater Quality 2001, Sheffield, UK, 2001; Sascha E. Oswald Steven F. Thornton, International Association of Hydrological Sciences: Sheffield, UK, 2001; p. 319-325.

16. Roberts, D. J. *Use of Landfarming to Remediate Soil Contaminated by Pesticides*. 1995, Springfield, IL: DIANE Publishing. p. 40-41.

17. California EPA. *In situ groundwater remediation at sites with volatile organic compounds, nitrogen compounds, perchlorate, pesticides, semi-volatile compounds and/or petroleum hydrocarbons*; State Water Resources Control Board, California EPA: CA, 2007; p. 1-8.

18. Matheson, L. J. and Tratnyek, P. G. *Reductive dehalogenation of chlorinated methanes by iron metal.* Environmental Science and Technology. **1994**, *28*, p. 2045-2053.

19. He, Y. T. and Traina, S. J. *Transformation of magnetite to goethite under alkaline pH conditions.* Clay Minerals. **2007**, *42*, p. 13-19.

20. Weber, E. J. *Iron-Mediated Reductive Transformations: Investigation of Reaction Mechanism.* Environmental Science and Technology. **1996**, *30*, p. 716-719.

21. Roberts, A. L.;Totten, L. A.;Arnold, W. A.;Burris, D. R. and Campbell, T. J. *Reductive elimination of chlorinated ethylenes by zero-valent metals.* Environmental Science and Technology. **1996**, *30*(8), p. 2654-2659.

22. Farrell, J.;Kason, M.;Melitas, N. and Li, T. *Investigation of the long-term performance of zero-valent iron for reductive dechlorination of trichloroethylene.* Environmental Science and Technology. **2000**, *34*(3), p. 512-521.

23. Liang, L.;Korte, N.;Gu, B.;Puls, R. and Reeter, C. *Geochemical and microbial reactions affecting the long-term performance of in situ "iron barriers".* Advances in Environmental Research. **2000**, *4*(4), p. 273-286.

24. Lai, K. C.-K. and Lo, I. M.-C. In *Field monitoring of the performance of a PRB at the Vapokon site, Denmark.*, Permeable Reactive Barriers (PBRs) Action Team Meeting, Niagara Falls, New York, October 15-16, 2003; Niagara Falls, New York, 2003.

25. Lai, K. C. K.;Lo, I. M. C. and Kjeldsen, P. In *Permeable Reactive Barriers*, 1st International Symposium on Permeable Reactive Barriers, Belfast, Northern Ireland, March 14-16, 2004; Genevieve A. Boshoff and Brian D. Bone, International Association of Hdyrological Sciences: Belfast, Northern Ireland, 2004; p. 12-22.

26. Jeffers, P. M.;Ward, L. M.;Woytowitch, L. M. and Wolfe, N. L. *Homogeneous hydrolysis rate constants for selected chlorinated methanes, ethanes, ethenes, and propanes.* Environmental Science and Technology. **1989**, *23*(8), p. 965-969.

27. McCormick, M. L. and Adriaens, P. *Carbon tetrachloride transformation on the surface of nanoscale biogenic magnetite particles.* Environmental Science and Technology. **2004**, *38*, p. 1045-1053.

28. Air Toxics Website: Chloroform. http://www.epa.gov/ttn/atw/hlthef/chlorofo.html . (July, 2010)

29. Xu, Y. and Zhang, W.-x. *Subcollodial Fe/Ag particles for reduction of chlorinated benzenes.* Industrial & Engineering Chemistry Research. **2000**, *39*, p. 2238-2244.

30. Bhandari, A.;Surampalli, R. Y.;Champagne, P.;Ong, S. K.;Tyagi, R. D. and Lo, I. M. C. *Remediation Technologies for Soils and Groundwater*. 2007, Reston, VA: ASCE Publications. p. 155-158.

31. Arnold, W. A. and Roberts, A. L. *Pathways of chlorinated ethylene and chlorinated acetylene reaction with Zn(O).* Environmental Science and Technology. **1998**, *32*(19), p. 3017-3025.

32. Liu, Y.;Majetich, S. A.;Tilton, R. D.;Sholl, D. S. and Lowry, G. V. *TCE dechlorination rates, pathways, and efficiency of nanoscale iron particles with different properties.* Environmental Science and Technology. **2005**, *39*(5), p. 1338-1345.

33. Wang, C.-B. and Zhang, W.-X. *Synthesizing nanoscale iron particles for rapid and complete dechlorination of TCE and PCBs.* Environmental Science and Technology. **1997**, *31*, p. 2154-2156.

34. Nurmi, J. T.;Tratnyek, P. G.;Sarathy, V.;Linehan, J. C.;Matson, D. W.;Penn, R. L. and Driessen, M. D. *Characterization and properties of metallic iron nanoparticles: Spectroscopy, electrochemistry, and kinetics.* Environmental Science and Technology. **2005**, *39*, p. 1221-1230.

35. Vikesland, P. J.;Heathcock, A. M.;Rebodos, R. L. and Makus, K. E. *Particle size and aggregation effects on magnetite reactivity toward carbon tetrachloride.* Environmental Science and Technology. **2007**, *41*, p. 5277-5283.

36. Bransfield, S. J.;Cwiertny, D. M.;Roberts, A. L. and Fairbrother, D. H. *Influence of copper loading and surface coverage on the reactivity of granular iron toward 1,1,1-trichloroethane.* Environmental Science and Technology. **2006**, *40*, p. 1485-1490.

37. Cwiertny, D. M.;Bransfield, S. J.;Livi, K. J. T.;Fairbrother, D. H. and Roberts, A. L. *Exploring the influence of granular iron additives on 1,1,1-trichloroethane reduction.* Environmental Science and Technology. **2006**, *40*, p. 6837-6843.

38. Cwiertny, D. M.;Bransfield, S. J. and Roberts, A. L. *Influence of the oxidizing species on the reactivity of iron-based bimetallic reductants.* Environmental Science and Technology. **2007**, *41*, p. 3734-3740.

39. Lien, H.-L. and Zhang, W.-x. *Hydrodechlorination of chlorinated ethanes by nanoscale Pd/Fe bimetallic particles.* Journal of Envrionmental Engineering. **2005**, *131*, p. 4-10.

40. Zhang, W.-X.;Wang, C.-B. and Lien, H.-L. *Treatment of chlorinated organic contaminants with nanoscale bimetallic particles.* Catalysis Today. **1998**, *40*, p. 387-395.

41. Lipczyska-Kochany, E.;Harms, S.;Milburn, R.;Sprah, G. and Nadarajah, H. *Degradation of carbon tetrachloride in the presence of iron and sulfur containing compounds.* Chemosphere. **1994**, *29*, p. 1477-1489.

42. Hofstetter, T. B.;Heijman, C. G.;Haderlein, S. B.;Holliger, C. and Schwarzenbach, R. P. *Complete reduction of TNT and other (poly)nitroaromatic compounds under iron-reducing subsurface conditions.* Environmental Science and Technology. **1999**, *33*, p. 1479-1487.

43. Klausen, J.;Troeber, S. P.;Haderlein, S. B. and Schwarzenbach, R. P. *Reduction of substituted nitrobenzenes by Fe(II) in aqueous mineral suspensions.* Environmental Science and Technology. **1995**, *29*, p. 2396-2404.

44. Devlin, J. F.;Klausen, J. and Schwarzenbach, R. P. *Kinetics of nitroaromatic reduction on granular iron in recirculating batch experiments.* Environmental Science and Technology. **1998**, *32*, p. 1941-1947.

45. Keum, Y.-S. and Li, Q. X. *Reduction of nitroaromatic pesticides with zero-valent iron.* Chemosphere. **2004**, *54*, p. 255-263.

46. Wetzel, R. G. *Limnology*. 2nd ed. 1983, Philadelphia: Saunders College Publishing. p. 261-263.

47. Rugge, K.;Hofstetter, T. B.;Haderlein, S. B.;Bjerg, P. L.;Knudsen, S.;Zraunig, C.;Mosbek, H. and Christensen, T. H. *Characterization of predominant reductants in an anaerobic leachate-contaminated aquifer by nitroaromatic probe compounds.* Environmental Science & Technology. **1998**, *32*(1), p. 23-31.

48. Elsner, M.;Schwarzenbach, R. P. and Haderlein, S. B. *Reactivity of Fe(II)-bearing minerals toward reductive transformation of organic contaminants.* Environmental Science and Technology. **2004**, *38*, p. 799-807.

49. Charlet, L.;Silvester, E. and Lifer, E. *N-compound reduction and actinide immobilisation in surficial fluids by Fe(II): the surface $Fe^{III}OFe^{II}OOH^{o}$ species, as major reductant.* Chemical Geology. **1998**, *151*, p. 85-93.

50. Klupinski, T. P.;Chin, Y.-P. and Traina, S. J. *Abiotic degradation of pentachloronitrobenzene by Fe(II): reactions on goethite and iron oxide nanoparticles.* Environmental Science and Technology. **2004**, *38*, p. 4353-4360.

51. Shultz, C. A. and Grundl, T. J. *pH dependence on reduction rate of 4-Cl-nitrobenze by Fe(II)/montmorillonite systems.* Environmental Science and Technology. **2000**, *34*, p. 3641-3648.

Chapter 2: Impact of Iron Salt Anion Identity on the Reactivity of Synthesized Iron Nanoparticles

2.1 Introduction

Zero-valent iron (ZVI) nanoparticles have emerged an effective reducing agent for halogenated contaminants. Highly oxidized contaminants are reduced when electrons are transferred from the ZVI to the contaminant. ZVI particles can be directly injected into contaminated groundwater sites or used in permeable reactive barriers *(1-5)*. Both methods have proven successful at reducing contaminants such as trichloroethene *(2, 3)*. Carbon tetrachloride (CT) is another groundwater contaminant that can be reduced by ZVI and is a known carcinogen regulated by the Safe Water Drinking Act with a maximum contaminant level (MCL) of 5 ppb *(6)*. Reduction of CT occurs by two potential pathways: hydrogenolysis and dichloroelimination *(6, 7)*. Hydrogenolysis results in the production of chloroform (CF), which can further degrade to dichloromethane. Dichloroelimination results in the formation of completely dehalogenated compounds, such as formate and carbon monoxide, via a dichlorocarbene intermediate *(6, 7)*. The branching ratio is used to describe the product yield from each of these mechanisms.

The addition of other metals to ZVI nanoparticles influences particle reactivity and product branching ratios. The addition of noble metals such as Pd, Pt, Ni, Ag, and Cu has been shown to increase rates of contaminant degradation *(8-14)*. Impurities in the materials used to produce ZVI and the presence of anions in solution can also influence particle reactivity. The presence of some impurities in iron, such as carbon, has been

shown to decrease ZVI particle reactivity *(13)*, while the presence of sulfur has been shown to enhance reactivity *(15, 16)*. Lipczyska-Kochany et al. *(16)* showed that using a combination of ZVI and iron sulfide greatly increases reactivity with respect to the rate of carbon tetrachloride reduction.

The presence of anions in solution also has an impact on ZVI reactivity. The anions SO_4^{2-}, Cl^-, NO_3^- and HCO_3^- have a varying impact on reactivity depending on the contaminant as well as the reactor conditions, such as pH and ionic strength *(17-19)*. Nitrate present in solution has been shown to inhibit reactivity at low pH values due to the formation of a FeOOH passivating layer around ZVI particles *(18, 19)*. Sulfate is thought to increase reactivity through formation of a layer of equally or more reactive material, such as iron sulfide *(17, 19)*. While the effect of impurities in the ZVI particles and of anions in the reaction media has been studied, there is less research examining the link between synthetic variables, such as counterions in reagent salts, with the reactivity of ZVI. The majority of past research focused on the presence of trace metals in cast iron *(6)* and iron containing minerals, such as pyrite *(16)*.

This study examined the effect of the identity of anions present during the synthesis of the iron oxyhydroxide used as the precursor to ZVI nanoparticles on the kinetics and branching ratio of CT reduction. The anions investigated were NO_3^-, Cl^-, SO_4^{2-}, and PO_4^{3-}. CT was used to test reactivity of the different materials, and CF was quantified to evaluate product branching ratios. ZVI particles were examined before and after reaction using powder x-ray diffraction (XRD), transmission electron microscopy

(TEM), TEM with energy dispersive x-ray spectroscopy (EDS), and x-ray photoelectron spectroscopy (XPS).

2.2 Materials and Methods

2.2.1 Materials

All reactions and material preparations were carried out in ultrapure 18MΩ•cm resistivity water (Milli-Q, Millipore). All Milli-Q water and solutions were deoxygenated by sparging with nitrogen gas. All glassware and Nalgene bottles were acid washed with 4 M HNO_3 and rinsed three times with Milli-Q water. Ferric nitrate ($Fe(NO_3)_3 \cdot 9H_2O$ crystalline, Fisher Chemical) and ferric chloride ($FeCl_3 \cdot H_2O$ lump, Fisher chemical) were both ACS grade and used as received. Ferric sulfate ($Fe_2(SO_4)_3 \cdot xH_2O$, 97% ACS grade) was purchased from Sigma-Aldrich. Potassium phosphate monobasic (KH_2PO_4 crystalline, ACS grade) and potassium hydroxide (KOH pellets, ACS grade) were purchased from J.T. Baker Chemical and Mallinckrodt Chemicals, respectively. High purity hydrogen, nitrogen, and gas mix ($95\%N_2/5\%H_2$) gas were purchased from Airgas Inc. MOPS (3-(N-morpholino)propanesulfonic acid, sodium salt) (>98% purity) was purchased from Fisher Scientific. Pentane (reagent grade) was purchased from Sigma-Aldrich.

2.2.2 Ferrihydrite Preparation

Ferrihydrite was used as the precursor to ZVI. The synthesis of the 2-line ferrihydrite particles was adapted from the procedure developed by Schwertman and

Cornell *(20)*. A 0.1 M Fe^{3+} aqueous solution was prepared by adding the appropriate amount of $Fe(NO_3)_3 \cdot 9H_2O$, $Fe_2(SO_4)_3$, or $FeCl_3 \cdot 6H_2O$. A 0.1 M Fe^{3+} solution was also prepared by adding the appropriate amount of $Fe(NO_3)_3 \cdot 9H_2O$ to a 0.01M KH_2PO_4 aqueous solution . Each individual solution was titrated with 0.1 M KOH until the pH was between 7 and 8. The freshly synthesized suspension was then transferred to 50 mL centrifuge tubes and centrifuged three times at 2604 rcf for 10 minute intervals using an Eppendorf Centrifuge 5804. The supernatant was discarded, and the particles were resuspended in fresh Milli-Q water. This procedure was repeated three times. The suspension was then placed in a Spectrum Labs Spectra-Por #7 dialysis bag and dialyzed against Milli-Q water for two days, changing the water six times. The suspended ferrihydrite particles were then transferred into plastic weigh boats, covered loosely, and allowed to dry. An agate mortar and pestle was used to grind the dried ferrihydrite into a fine powder, which was transferred to and stored in a glass vial.

Six-line ferrihydrite (6L-Fh) was synthesized by the process described by Erbs et. al. *(21)* For ease of further discussion each ferrihydrite sample will be described using the following notation: $Fh_{nL\text{-}anion}$. For example, the 2-line ferryhydrite prepared using nitrate is identified as $Fh_{2L\text{-}nitrate}$.

2.2.3 ZVI Preparation

A 1.5 g sample of each ferrihydrite sample was reground using an agate mortar and pestle. The ground sample was then reduced in a quartz tube furnace under H_2 gas with a flow rate of 100 mL min^{-1}. The furnace was maintained at 25 °C for 30 minutes

then heated to 450°C at a rate of 5°C min^{-1}. The furnace was then maintained at 450°C for 4 hours. The sealed tube was then transferred to an anaerobic chamber (Coy Laboratory Products, 5% H_2/95% N_2) where the material was reground and stored in a glass vial. The particles derived from $Fe_2(SO_4)_3$ or $Fe(NO_3)_3 \cdot 9H_2O$ with 0.01M KH_2PO_4 were treated by the reduction process a total a three times each to maximize reduction of the ferrihydrite to zero valent iron. The other ferrihydrite particles were treated via the reduction process one time. Particles were examined by XRD (described below) after each reduction trial to confirm the reduction of the ferrihydrite to ZVI. For ease of further discussion, ZVI samples will be identified using the following notation: $ZVI_{nL\text{-}Fh\text{-}anion}$.

2.2.4 Materials Characterization

XRD data were collected using a PANalytical X-Pert PRO MPD X-ray diffractometer equipped with a cobalt source and an X-Celerator detector over the range of 25-105° 2θ at a scan rate of 0.0235° per second. Samples were prepared for analysis in an anaerobic glove bag in air-tight sample holders. Diffraction patterns were compared to reference powder diffraction files (PDF) for iron (#6-0696), magnetite (#19-0629), goethite (#29-0713), vivianite (#30-0662), pyrrhotite (#22-1120), troilite (1-089-4076), and rockbridgeite (34-0150). Quantitative phase compositions were determined by Rietveld refinement *(22)* using the X-Pert High Score Plus (version 2.0.1) software and the known crystal structure data for the crystalline materials identified by XRD *(23-*

28). Data was plotted as the square root of intensity to better discern smaller peaks from minor phases.

TEM and TEM with EDS were performed using a FEI Technai G^2 F30 and FEI Technai T12. Particles were dry-mounted onto 3 mm 200-mesh holey carbon-coated copper grids (Structure Probe, Inc.) in the anaerobic glove bag and stored in an air-tight container until mounted onto the TEM sample holder. XPS was performed using EMSL, a national scientific user facility sponsored by the Department of Energy's Office of Biological and Environmental Research located at Pacific Northwest National Laboratory. XPS measurements were performed using a Physical Electronics Quantum 2000 Scanning ESCA Microprobe. This system used a focused monochromatic Al Kα x-rays (1486.7 eV) source and a spherical section analyzer. The instrument has a 16 element multichannel detector. The X-ray beam used was a 100 W, 100 mm diameter beam that was rastered over a 1.3 mm by 0.2 mm rectangle on the sample. The X-ray beam was incident normal to the sample and the photoelectron detector was at 45° off-normal. Wide scan data was collected using a pass energy of 117.4 eV. The high energy resolution photoemission spectra was collected using a pass energy of 46.95. The sample experienced variable degrees of charging. Low energy electrons at ~1 eV, 20μA and low energy Ar+ ions were used to minimize this charging.

2.2.5 Carbon Tetrachloride Reactors

Experiments were performed in 124 mL serum bottles without headspace. Each reactor contained 150 mg of solid sample weighed directly into the bottle. Reactions were initiated by adding the appropriate amount of 150 μM carbon tetrachloride (CT) solution prepared with pH 7.0 50 mM MOPS buffer. Reactors were capped with PTFE-lined septa and aluminum crimp caps and were covered in aluminum foil. Reactors were assembled in the anaerobic glove bag. After preparation, reactors were removed from the glove bag and mixed around their longitudinal axes on a Glas-Col rotator (50 rpm) at 22 ±2 ºC. Samples were withdrawn at desired time intervals by injecting deoxygenated buffer to avoid the introduction of headspace in the reactor.

CT and CF were analyzed using a gas chromatograph GC with a flame ionization detector or electron capture detector (Trace GC 2000, Thermoquest). Samples analyzed by flame ionization detection were 0.5 mL in volume and filtered using 0.2-μm nylon Acrodisc filters into 2.5-mL vials. Samples analyzed by electron capture detection were 10 μL in volume and were extracted into GC vials containing 1 mL of pentane. All samples were capped with a PTFE-lined septum and an aluminum crimp cap. Samples analyzed by the flame ionization detector were incubated at 40 ºC for 25 minutes. Next a 250 μL headspace sample was injected (splitless, 150 ºC) by an HS 2000 headspace autosampler (ThermoQuest) onto a GS-GasPro Column (30 m × 0.32 mm i.d., J&W Scientific) using He carrier gas at 60 kPa. The oven temperature was initially held at 40 ºC for 1 minute, increased to 130 ºC at a rate of 20 ºC/minute, increased to 210 ºC at a rate of 5 ºC/minute, increased to 240 ºC at a rate of 25 ºC/minute, and finally held for 1

minute at 240 ºC. For samples analyzed by the electron capture detector a 2 µL sample was injected by an AS 2000 autosampler (Thermoquest) onto a GS-GasPro column (30 m × 0.32 mm i.d., J&W Scientific) using helium as the carrier gas at 60 kPa and argon/methane as the detector makeup gas at 30 mL/min. The temperature was held at 40 °C for 5 minutes, increased at a rate of 10 °C per minute to 120 °C followed by a rate of 30 °C per minute to 240 °C with a 1 minute hold at 240 °C. Six-point calibration curves were used to quantify the concentration of CT and CF. Standards were prepared by dilution of CT and CF methanolic stock solutions into pH 7.0 50 mM MOPS buffer in serum bottles, which were then treated in the same manner as samples. After reaction ZVI particles were dried under N_2 and collected to characterize the solids. Respike experiments were performed for each particle set 24 hours after the first CT spike. Respike reactions were carried out as described above.

The degradation of CT from reaction with ZVI was modeled as a pseudo-first order reaction. Only the concentrations of CT and CF were quantified in this study. The reactions considered and their rate constants of interest are shown by Equations 2-1 and 2-2.

$$CCl_4 \xrightarrow{k_1} CCl_3H \xrightarrow{k_2} CCl_2H_2 \qquad (2\text{-}1)$$

$$CCl_4 \xrightarrow{k_3} \text{other products} \qquad (2\text{-}2)$$

The other products refer to methane, carbon monoxide, and formate, which were not quantified in these experiments. The chloroform yield was calculated as follows:

$$Y_{CF} = \frac{k_1}{k_1 + k_3} \quad (2\text{-}3)$$

Scientist for Windows (Micromath Scientific Software, v.2.1, USA) was used to calculate reaction rate constants by fitting the kinetic data to the differential rate expressions.

Reactions were also performed in the absence of CT to observe the aging effects of the buffer solution on the particles. Reactions were carried out as described above with the exception of the CT addition to the reactors. Particles were collected after reaction and dried under N_2 for characterization.

2.3 Results and Discussion

2.3.1 Characterization of Solid Materials: Pre-reaction

The XRD patterns for all ZVI particles are shown in Figure 2-1, and results from the Rietveld refinement of each XRD pattern are presented in Table 2-1. Rietveld refinement of the XRD patterns was used to determine the percentage by weight of each component present in the ZVI starting materials. All samples were mostly reduced to ferrite (i.e. ZVI) with trace amounts of magnetite (Fe_3O_4). The magnetite peaks were most likely not visible in the $ZVI_{2L\text{-}Fh\text{-}nitrate}$ and $ZVI_{2L\text{-}Fh\text{-}chloride}$ XRD patterns due to the strong presence of the ferrite peaks. The refinement detection limit for a phase is 1 wt%, so the amount of magnetite present for all particle sets is approximately 1 wt%. Iron sulfide, troilite (FeS), was detected in the $ZVI_{2L\text{-}Fh\text{-}sulfate}$ sample. $ZVI_{2L\text{-}Fh\text{-}phosphate}$ contained a variety of compounds in addition to ferrite, including iron phosphide, iron

phosphate, phosphorus and phosphorus oxide. Numerous additional small peaks were also detected, but they could not be identified by comparison to the PDF (powder diffraction file) database. The iron phosphate rockbridgiete ($Fe^{2+}Fe_4^{3+}[(OH)_5|(PO_4)_3]$) was the only material present in the $ZVI_{2L\text{-}Fh\text{-}phosphate}$ that was able to be refined. The presence of additional materials such as troilite and iron phosphate, in $ZVI_{2L\text{-}Fh\text{-}sulfate}$ and $ZVI_{2L\text{-}Fh\text{-}phosphate}$ respectively, could interfere with the reduction of the ferrihydrite to ZVI, resulting in materials that are not fully reduced. Finally, XRD results were also used to calculate the average particle size using the Scherrer equation. The averages were in the 100-200 nm range in diameter and were, thus, not significantly different from each other.

TEM images and electron diffraction patterns confirmed the XRD findings. Figure 2-2 shows representative images of $ZVI_{2L\text{-}Fh\text{-}nitrate}$, $ZVI_{2L\text{-}Fh\text{-}chloride}$, $ZVI_{2L\text{-}Fh\text{-}sulfate}$, and $ZVI_{2L\text{-}Fh\text{-}phosphate}$. Neither nitrogen in $ZVI_{2L\text{-}Fh\text{-}nitrate}$ nor chloride in $ZVI_{2L\text{-}Fh\text{-}chloride}$ was detected. In contrast, sulfur was detected in the $ZVI_{2L\text{-}Fh\text{-}sulfate}$, as was phosphorus in the $ZVI_{2L\text{-}Fh\text{-}phosphate}$. A thin oxide layer was clearly discernible only in images of $ZVI_{2L\text{-}Fh\text{-}chloride}$. This oxide layer was possibly formed during the transfer of the particles from their air-tight container to the TEM sample holder and into the instrument or was a result of incomplete reduction. Both $ZVI_{2L\text{-}Fh\text{-}nitrate}$ and $ZVI_{6L\text{-}Fh\text{-}nitrate}$ were indistinguishable in TEM images as well as by EDS analysis. TEM analysis showed particles in all sets were 100-200 nm in diameter, which is consistent with XRD results.

XPS results provided information on particle composition and the oxidation states of sulfur, phosphorus and iron before and after reaction with CT. Sodium was detected in pre-reaction $ZVI_{2L\text{-}Fh\text{-}chloride}$ and $ZVI_{2L\text{-}Fh\text{-}phosphate}$. Chloride was present in very small

amounts (less than 0.7 mol %) in $ZVI_{2L\text{-}Fh\text{-}nitrate}$ and in $ZVI_{2L\text{-}Fh\text{-}chloride}$ (~1 mol %). Sulfur was present only in the pre-reaction $ZVI_{2L\text{-}Fh\text{-}sulfate}$. Oxygen was present before reaction in all materials. High energy resolution photoemission spectra detected both Fe^{II} and

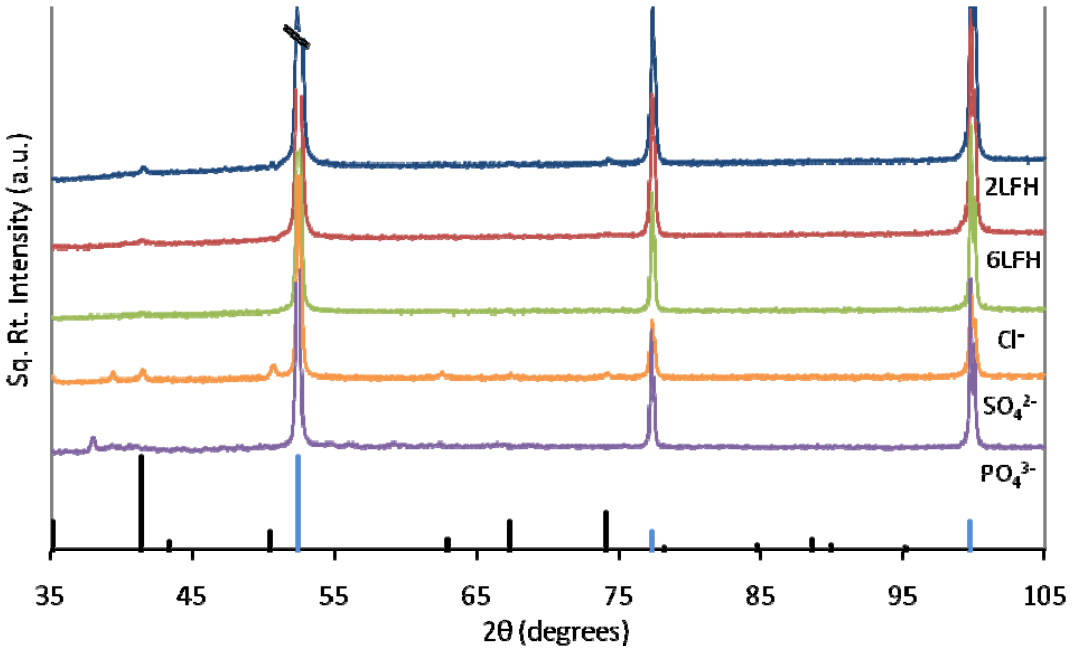

Figure 2-1. Powder XRD data for all ZVI particle sets compared with PDF reference patterns for ferrite and magnetite. The ferrite peak at 2θ of 52° has been cut down to make minor peaks visible.

Fe^{III}, which were likely due to oxidation of the particle surfaces during analysis. ZVI was only detected in $ZVI_{2L\text{-}Fh\text{-}nitrate}$ after reaction and $ZVI_{2L\text{-}Fh\text{-}chloride}$ before reaction. ZVI, however, is known to be present in all pre- and post-reaction particles based on XRD and TEM data. XPS is a surface sensitive technique, and therefore oxidation on the surface of the particles would shield the ZVI core from detection.

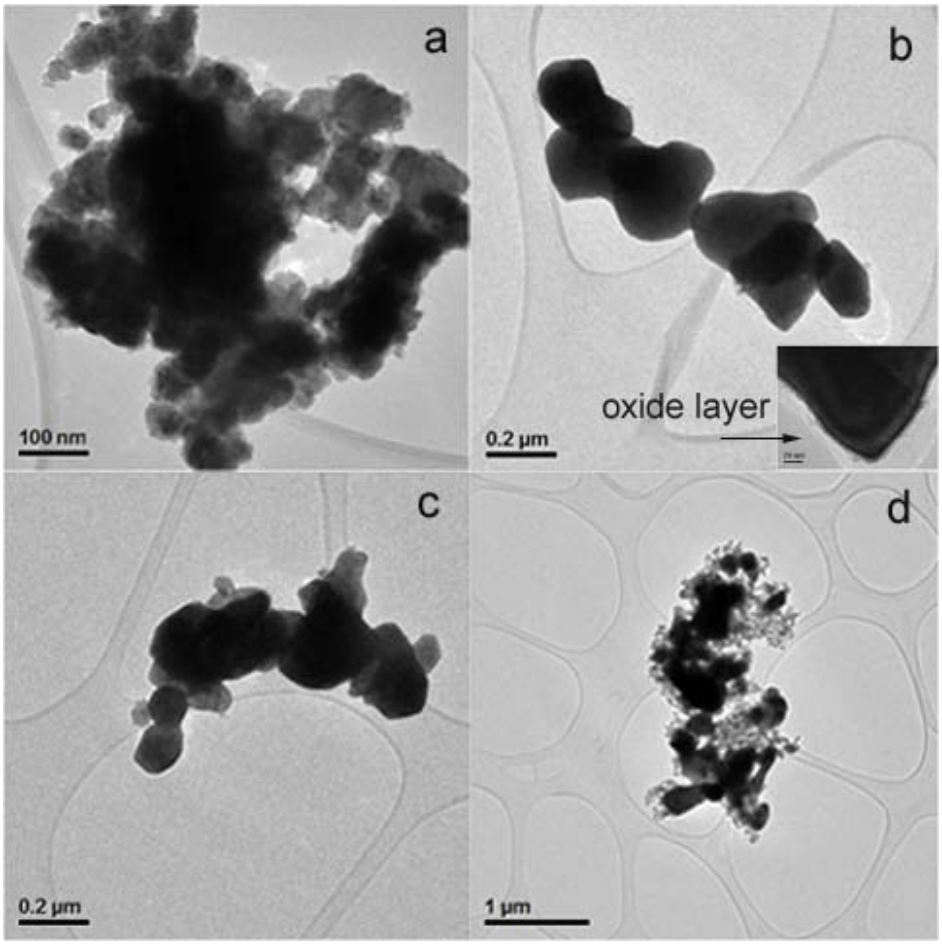

Figure 2-2. TEM images of ZVI particles: a) $ZVI_{2L\text{-}Fh\text{-}nitrate}$ b) $ZVI_{2L\text{-}Fh\text{-}chloride}$ c) $ZVI_{2L\text{-}Fh\text{-}sulfate}$ d) $ZVI_{2L\text{-}Fh\text{-}phosphate}$

Table 2-1. Rietveld refinement results quantifying the minerals present for each particle set.

	Average Material %								
	Ferrite Fe^0	Magnetite Fe^3O^4	Goethite α- FeOOH	Troilite FeS	Rockbridgeite $Fe^{2+}Fe_4^{3+}[(OH)_5\|(PO_4)_3]$	Pyrrhotite $Fe_{1-x}S$	Vivianite $Fe^{2+}{}_3(PO_4)_2 \cdot H_2O$	GOF[a]	WRP[b]
Before reaction with CT									
$ZVI_{2L\text{-}Fh\text{-}nitrate}$	98.8	1.2	0.0	0.0	0.0	0.0	0.0	9.9	2.9
$ZVI_{6L\text{-}Fh\text{-}nitrate}$	98.5	1.5	0.0	0.0	0.0	0.0	0.0	5.9	2.6
$ZVI_{2L\text{-}Fh\text{-}chloride}$	98.5	1.5	0.0	0.0	0.0	0.0	0.0	3.2	2.5
$ZVI_{2L\text{-}Fh\text{-}sulfate}$	91.6	5.2	0.0	3.2	0.0	0.0	0.0	6.1	2.2
$ZVI_{2L\text{-}Fh\text{-}phosphate}$	97.4	0.2	0.0	0.0	2.4	0.0	0.0	3.9	2.9
After reaction with CT									
$ZVI_{2L\text{-}Fh\text{-}nitrate}$	4.7	88.7	6.7	0.0	0.0	0.0	0.0	5.1	3.2
$ZVI_{6L\text{-}Fh\text{-}nitrate}$	36.7	55.3	8.1	0.0	0.0	0.0	0.0	7.9	3.8
$ZVI_{2L\text{-}Fh\text{-}chloride}$	28.2	67.5	4.3	0.0	0.0	0.0	0.0	4.7	2.9
$ZVI_{2L\text{-}Fh\text{-}sulfate}$	2.5	87.0	0.0	0.0	0.0	10.5	0.0	7.1	3.5
$ZVI_{2L\text{-}Fh\text{-}phosphate}$	32.7	26.9	0.0	0.0	0.0	0.0	40.4	4.5	3.2
After reaction without CT									
$ZVI_{2L\text{-}Fh\text{-}nitrate}$	42.2	57.8	0.0	0.0	0.0	0.0	0.0	6.9	3.0
$ZVI_{2L\text{-}Fh\text{-}chloride}$	54.4	45.6	0.0	0.0	0.0	0.0	0.0	5.8	2.6
$ZVI_{2L\text{-}Fh\text{-}sulfate}$	23.2	68.5	0.0	0.0	0.0	8.2	0.0	8.4	3.8
$ZVI_{2L\text{-}Fh\text{-}phosphate}$	94.5	0.0	0.0	0.0	0.0	0.0	6.5	5.5	3.3

a. GOF: Goodness of fit.

b. WRP: Weighted R-profile.

2.3.2 CT Degradation Kinetics and Pathways

Table 2-2 presents the calculated rate constants and chloroform yields. The overall CT degradation rate constant is given by k_{obs}, which is the sum of k_1 and k_3 with appropriate error propagation. The rate constant k_2 was set to zero for all materials because little to no CF degradation was observed over the 6 hour sampling period for these experiments. The overall k_{obs} for the $ZVI_{2L\text{-}Fh\text{-}nitrate}$, $ZVI_{6L\text{-}Fh\text{-}nitrate}$, and $ZVI_{2L\text{-}Fh\text{-}chloride}$ particles were similar and were slowest of all the materials. The k_{obs} for $ZVI_{2L\text{-}Fh\text{-}sulfate}$ was approximately twice that of the $ZVI_{2L\text{-}Fh\text{-}nitrate}$, $ZVI_{6L\text{-}Fh\text{-}nitrate}$ and $ZVI_{2L\text{-}Fh\text{-}chloride}$, while k_{obs} for $ZVI_{2L\text{-}Fh\text{-}phosphate}$ was four times that of the $ZVI_{2L\text{-}Fh\text{-}nitrate}$, $ZVI_{6L\text{-}Fh\text{-}nitrate}$ and $ZVI_{2L\text{-}Fh\text{-}chloride}$.

Examining the corresponding chloroform yields reveals a similar trend to the rate constants. $ZVI_{2L\text{-}Fh\text{-}nitrate}$, $ZVI_{6L\text{-}Fh\text{-}nitrate}$ and $ZVI_{2L\text{-}Fh\text{-}chloride}$ had the lowest chloroform yields, around 20%. $ZVI_{2L\text{-}Fh\text{-}sulfate}$ and $ZVI_{2L\text{-}Fh\text{-}phosphate}$ had chloroform yields of approximately 50% and 90%, respectively. Plots of CT concentration vs. time data for each particle type are shown in Figure 2-3. The majority of the CT was degraded within two hours, and the differences in the concentrations of CF formed are easily visible when comparing the $ZVI_{2L\text{-}Fh\text{-}sulfate}$ and $ZVI_{2L\text{-}Fh\text{-}phosphate}$ particles to the $ZVI_{2L\text{-}Fh\text{-}nitrate}$, $ZVI_{6L\text{-}Fh\text{-}nitrate}$ and $ZVI_{2L\text{-}Fh\text{-}chloride}$. From the perspective of kinetics, this suggests that the addition of sulfate or phosphate produces a more reactive ZVI. From the perspective of chloroform yield, this suggests that the addition of sulfate or phosphate is not desirable. While these two anions lead to increased reaction rates, the production of chloroform was significantly increased with no degradation of the chloroform observed.

Table 2-2. Rate constants for reaction of CT with ZVI.[a]

Particle Type	k_1	k_2	k_3	k_{obs}	Y_{CF}
$ZVI_{2L\text{-}Fh\text{-}nitrate}$	0.27 ± 0.06[b]	0.0	1.1 ± 0.18	1.3 ± 0.33	0.20 ± 0.087
$ZVI_{6L\text{-}Fh\text{-}nitrate}$	0.50 ± 0.14	0.0	1.4 ± 0.44	1.9 ± 0.65	0.27 ± 0.12
$ZVI_{2L\text{-}Fh\text{-}chloride}$	0.31 ± 0.070	0.0	1.1± 0.20	1.4 ± 0.37	0.22 ± 0.082
$ZVI_{2L\text{-}Fh\text{-}sulfate}$	1.0 ± 0.06	0.0	1.0 ± 0.15	2.1 ± 0.28	0.50 ± 0.057
$ZVI_{2L\text{-}Fh\text{-}phosphate}$	3.3 ± 0.15	0.0	0.48 ± 0.24	3.77 ± 0.49	0.87 ± 0.082

[a]Rate constants, with units h^{-1}, are averages from triplicate.
[b]Errors are 95% confidence intervals.

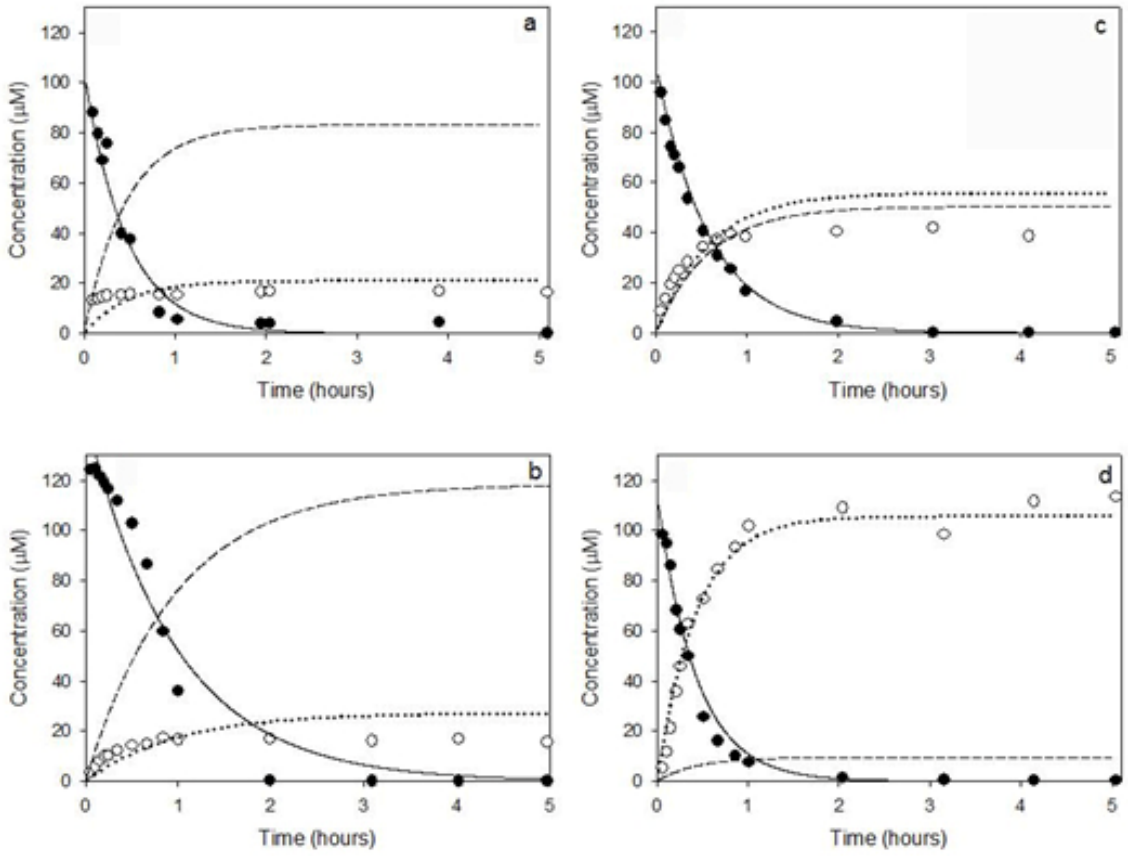

Figure 2-3. CT (●) degradation by ZVI and subsequent CF (○) formation: a) $ZVI_{2L\text{-}Fh\text{-}nitrate}$ b) $ZVI_{2L\text{-}Fh\text{-}chloride}$ c) $ZVI_{2L\text{-}Fh\text{-}sulfate}$ d) $ZVI_{2L\text{-}Fh\text{-}phosphate}$. Lines are model fits for CT (___), CF (·····) and other products (-----).

2.3.3 Characterization of Solid Materials: Post-Reaction

ZVI materials were also characterized after reaction with CT using XRD (Figure 2-4; Table 2-1) and TEM (Figure 2-5). A variety of solid phases formed. Post-reaction $ZVI_{2L\text{-}Fh\text{-}nitrate}$, $ZVI_{6L\text{-}Fh\text{-}nitrate}$, and $ZVI_{2L\text{-}Fh\text{-}chloride}$ contained ferrite (Fe^0), magnetite and goethite (α-FeOOH). Post-reaction $ZVI_{2L\text{-}Fh\text{-}sulfate}$ contained ferrite, magnetite, and pyrrhotite ($Fe_{1\text{-}x}S$). Finally, post-reaction $ZVI_{2L\text{-}Fh\text{-}phosphate}$ contained ferrite, magnetite, and vivianite ($Fe^{2+}_3(PO_4)_2 \cdot H_2O$). In addition, several small peaks in the post-reaction $ZVI_{2L\text{-}Fh\text{-}phosphate}$ XRD pattern indicate the presence of one or more crystalline materials, but these peaks could not be successfully matched to known materials in the PDF database. Only ferrite, magnetite and vivianite were considered for the Rietveld refinement of $ZVI_{2L\text{-}Fh\text{-}phosphate}$ particles for ease of refinement.

The amount of ferrite consumed during reaction varied depending upon the sample preparation conditions. Post-reaction $ZVI_{2L\text{-}Fh\text{-}nitrate}$ and $ZVI_{2L\text{-}Fh\text{-}sulfate}$ had approximately 2-5 wt % ZVI remaining compared to approximately 30 wt % for the other three materials. This could suggest that the other preparations might produce materials with a longer useful life in the field. For each of the aforementioned samples, magnetite was the dominant phase present after reaction. Goethite was formed in the $ZVI_{2L\text{-}Fh\text{-}chloride}$, $ZVI_{2L\text{-}Fh\text{-}nitrate}$, and $ZVI_{6L\text{-}Fh\text{-}nitrate}$, in order of increasing wt % goethite. Vivianite and pyrrhotite were detected in post-reaction $ZVI_{2L\text{-}Fh\text{-}phosphate}$ and $ZVI_{2L\text{-}Fh\text{-}sulfate}$, respectively.

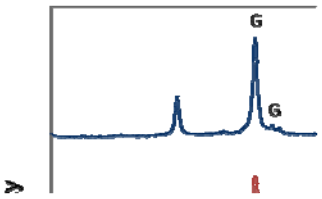

Figure 2-4. XRD patterns for ZVI particles post-reaction with CT compared to ferrite and magnetite PDF reference patterns. Goethite (G), pyrrhotite (P) and vivianite (V) peaks are labeled.

TEM images and electron diffraction patterns of the post-reaction particles were consistent with the XRD results. EDS results showed that the distribution of sulfur and phosphorus in $ZVI_{2L\text{-}Fh\text{-}sulfate}$ and $ZVI_{2L\text{-}Fh\text{-}phophate}$, respectively, were heterogeneous. Figure 2-5 shows images of particles after reaction along with EDS collected from different areas of the post-reaction $ZVI_{2L\text{-}Fh\text{-}phosphate}$, which show the heterogeneous distribution of phosphorus. All post-reaction materials appeared to be predominantly comprised of either magnetite, pyrrhotite or vivianite, depending on the starting material. Copper peaks shown by EDS were from the TEM grid.

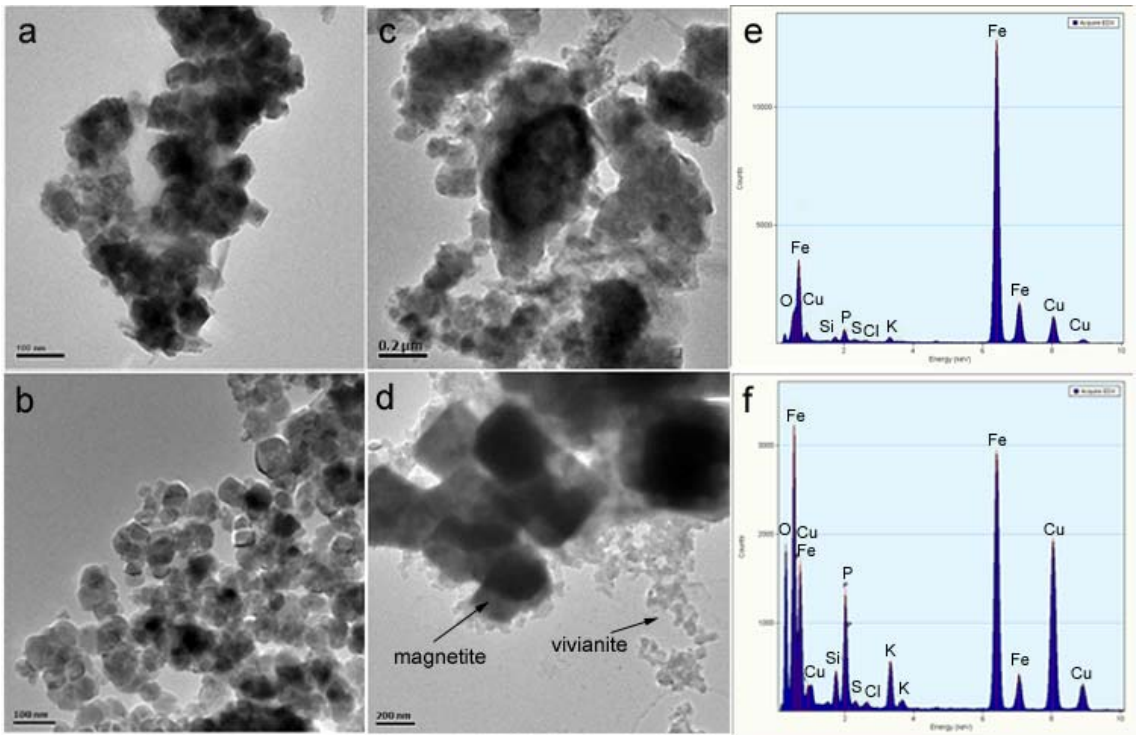

Figure 2-5. TEM images of ZVI particles after reaction with CT: Particles synthesized in the presnce of: a) NO_3^- (2LFH) b) Cl^- c) SO_4^{2-} d) PO_4^{3-}; EDS from areas of image d: e) magnetite area f) vivianite area

XPS results indicated that sulfur was present in the pre-reaction $ZVI_{2L\text{-}Fh\text{-}sulfate}$ and in all post-reaction materials, although the highest sulfur concentration was detected in the pre- and post-reaction $ZVI_{2L\text{-}Fh\text{-}sulfate}$. Wulfur, in the form of sulfate and sulfone, and sodium were detected after reaction in all particle sets. This is most likely due to incomplete removal of MOPS buffer after harvesting post-reaction materials from reactors. Post-reaction materials were rinsed with Milli-Q water and acetone before drying, but it is likely that the buffer was not completely removed by this procedure. Phosphorus was present before and after reaction in $ZVI_{2L\text{-}Fh\text{-}phosphate}$ and decreased by approximately 6 mol % during reaction. Additional forms of phosphorus were not identified by XPS. Reaction with CT led to the formation of iron phosphate in $ZVI_{2L\text{-}Fh\text{-}}$

$_{phosphate}$, coinciding with the detection of the iron phosphate vivianite by XRD. The formation of iron phosphate could explain the reduction in phosphorus detected by XPS. High energy resolution photoemission spectra provided qualitative comparisons between Fe^{II} and Fe^{III}. Fe^{II} increased in all samples after reaction, while Fe^{III} appeared to decrease slightly in the $ZVI_{2L\text{-}Fh\text{-}nitrate}$ and $ZVI_{2L\text{-}Fh\text{-}chloride}$. Fe^{III} increased after reaction in the $ZVI_{2L\text{-}Fh\text{-}phosphate}$ and was unchanged in the $ZVI_{2L\text{-}Fh\text{-}sulfate}$. The increase in Fe^{II} in post-reaction materials is due to the oxidation of ZVI to magnetite.

2.3.4 Characterization of Solid Materials: Blanks (no CT)

Blank reactions were also performed without the addition of CT to determine the aging effects of the buffer on the particles. When the particles were aged in the buffer solution, the solid products formed were different than those formed when CT was present. This indicates that the reaction products formed are influenced by reaction with CT. Table 2-1 lists the Rietveld refinement results from each particle set after the blank reaction. Most notable was the absence of the formation of goethite for $ZVI_{2L\text{-}Fh\text{-}nitrate}$, $ZVI_{6L\text{-}Fh\text{-}nitrate}$, and $ZVI_{2L\text{-}Fh\text{-}chloride}$. The amount of ZVI remaining in the material after aging in the buffer solution was much higher than that of the post-CT reaction materials. Notably, the amount of ZVI remaining in post-blank-reaction $ZVI_{2L\text{-}Fh\text{-}phosphate}$ was over 90%, which could suggest that the addition of phosphorous produced a material that is far more selective in the sense that very little oxidation was observed in the absence of CT.

2.3.5 Respike Experiments

The type of solid products formed during reaction could have an effect on the reactivity of the particles over time. Respike experiments with all of the ZVI materials revealed a significant drop in reactivity. Very little to no degradation of CT was observed after respike of CT into the reactors, even after 6 hours. Rate constants for the degradation of CT (k_{obs}) ranged from 0.14 ± 0.031 h^{-1} for $ZVI_{2L\text{-}Fh\text{-}chloride}$ and -.069 ± 0.025 h^{-1} for $ZVI_{2L\text{-}Fh\text{-}nitrate}$ to 0.14 ± 0.065 h^{-1} for $ZVI_{2L\text{-}Fh\text{-}sulfate}$ and 0.39 ± 0.032 h^{-1} for $ZVI_{2L\text{-}Fh\text{-}phosphate}$. No degradation of CT was observed for $ZVI_{2L\text{-}Fh}$-nitrate and the concentration data fluctuated, likely causing the negative rate constant. CF degradation (k_2) were again set to zero as no degradation of CF was observed. The degradation rate of CT did not appear to correlate with the remaining wt % iron. $ZVI_{2L\text{-}Fh\text{-}phosphate}$ had significantly less wt % magnetite after reaction as compared to the other materials. Magnetite is much less reactive than ZVI, and therefore could result in decreased reaction rates with CT as a magnetite layer forms over the particles. This could account for the higher k_{obs} value observed for $ZVI_{2L\text{-}Fh\text{-}phosphate}$, as there was less magnetite to slow the reduction of CT by iron metal.

2.3.6 Implications of Iron Nanoparticle Preparation on Chlorinated Solvent Degradation

None of the ferrihydrite precursor samples were completely reduced to ZVI during the hydrogen reduction process. It is possible full reduction could be achieved by using additional cycles of hydrogen reduction treatments, as were used with $ZVI_{2L\text{-}Fh\text{-}sulfate}$

and $ZVI_{2L\text{-}Fh\text{-}phosphate}$ particle sets. The gains in reactivity achieved by reducing the remaining magnetite, however, would probably be minimal, for oxidation of the ZVI would begin immediately upon exposure to the reaction medium. The exception may be $ZVI_{2L\text{-}Fh\text{-}phosphate}$, which contained barely detectable magnetite in pre-reaction and post-blank samples. Thus, the incorporation of phosphorous may yield a ZVI that is more resistant to oxidation in the absence of chlorinated solvent molecules. $ZVI_{2L\text{-}Fh\text{-}sulfate}$ and $ZVI_{2L\text{-}Fh\text{-}phosphate}$ also both contained materials other than ZVI and magnetite. The presence of additional materials such as troilite and iron phosphate, in $ZVI_{2L\text{-}Fh\text{-}sulfate}$ and $ZVI_{2L\text{-}Fh\text{-}phosphate}$ respectively, could interfere with the reduction of the ferrihydrite to ZVI, resulting in materials that are not fully reduced.

There are several possibilities for the observed effects on the particle reactivity. The presence of different minerals in the pre-reaction ZVI could have an effect on particle reactivity. Another possible difference is the relative amount of each type of crystal surface present in each sample, and subtle differences in particle morphology that could escape detection by conventional TEM but have substantial effects on the reactivity of the ZVI particles. It is also possible that the surfaces of the in $ZVI_{2L\text{-}Fh\text{-}sulfate}$ and $ZVI_{2L\text{-}Fh\text{-}phosphate}$ are different than the $ZVI_{2L\text{-}Fh\text{-}nitrate}$, $ZVI_{6L\text{-}Fh\text{-}nitrate}$ and $ZVI_{2L\text{-}Fh\text{-}chloride.}$ The presence of minerals such as iron sulfide and iron phosphate may have influenced reduction of the ferrihydrite to ZVI, resulting in differences in the atomic planes, or crystal surfaces, present on the ZVI particle surface. Different crystal surfaces could influence reactivity, resulting in increased degradation rates as observed for the $ZVI_{2L\text{-}Fh\text{-}sulfate}$ and $ZVI_{2L\text{-}Fh\text{-}phosphate}$. There may also be a thin layer of more reactive material, such

as iron sulfide, around particles that was not observed by TEM, which could influence reaction rates and pathways.

The anions present during ferrihydrite synthesis also affected the solid phase products. $ZVI_{2L\text{-}Fh\text{-}nitrate}$, $ZVI_{6L\text{-}Fh\text{-}nitrate}$, and $ZVI_{2L\text{-}Fh\text{-}chloride}$ particles contained magnetite and goethite after reaction with CT. Goethite was not detected in post-reaction $ZVI_{2L\text{-}Fh\text{-}sulfate}$ nor $ZVI_{2L\text{-}Fh\text{-}phosphate}$. Formation of iron sulfides and iron phosphates occurred in each of these particle sets, respectively. The type of solid products formed during reaction could have an effect on the reactivity of the particles over time. Iron sulfides have been found to be more reactive than magnetite *(40)*, which could explain the increased reactivity of the $ZVI_{2L\text{-}Fh\text{-}sulfate}$, as compared to the $ZVI_{6L\text{-}Fh\text{-}nitrate}$, $ZVI_{2L\text{-}Fh\text{-}nitrate}$ and $ZVI_{2L\text{-}Fh\text{-}chloride}$. Hydrolysis of $FeSO_4$ forms ferric hydroxides and generates sulfate ions, which are known to remove iron oxides and hydroxides that have formed on an iron surface *(40)*. This process could inhibit the growth of a corrosion layer around the $ZVI_{2L\text{-}Fh\text{-}sulfate}$ surfaces, allowing for faster reaction rates with CT. It is possible that the phosphate ions have a similar effect in that they prevent the formation of a corrosion layer around the $ZVI_{2L\text{-}Fh\text{-}phosphate}$ particles. The amount of ZVI present after reaction varies between each sample. This suggests that the accessibility of the ZVI is different for each particle set, which could be a result of the presence of different minerals in each of the types of particles.

Reaction of the ZVI materials with CT indicated significant differences in particle reactivity and CT degradation product distribution. Alpha elimination is the dominant reaction mechanism for $ZVI_{2L\text{-}Fh\text{-}nitrate}$, $ZVI_{6L\text{-}Fh\text{-}nitrate}$ and $ZVI_{2L\text{-}Fh\text{-}chloride}$. Examination of

k_1, however, indicates that hydrogenolysis is the more important reaction pathway for the $ZVI_{2L\text{-}Fh\text{-}sulfate}$ particles and $ZVI_{2L\text{-}Fh\text{-}phosphate}$ particles. Rate constants for $ZVI_{2L\text{-}Fh\text{-}sulfate}$ and $ZVI_{2L\text{-}Fh\text{-}phosphate}$ were 1.5 to 3 times higher than those for $ZVI_{2L\text{-}Fh\text{-}nitrate}$, $ZVI_{6L\text{-}Fh\text{-}nitrate}$ and $ZVI_{2L\text{-}Fh}$-chloride. This results in the formation of large quantities of chloroform as compared to the $ZVI_{2L\text{-}Fh\text{-}nitrate}$, $ZVI_{6L\text{-}Fh\text{-}nitrate}$ and $ZVI_{2L\text{-}Fh\text{-}chloride}$. This suggests that the presence of iron sulfide and iron phosphides and phosphates in ZVI materials influences not only the reaction rate, but also the reaction pathway of CT. This also suggests that if ZVI nanoparticles were used for remediation purposes, particles prepared in the presence of sulfate and phosphate have a limitation in that there is a high yield of chloroform, despite the faster CT degradation kinetics.

It is also noteworthy that no significant degradation of CF was observed. This is in stark contrast to the results from experiments employing bimetallic particles. In some of those cases, such as bimetallic Fe-Cu particles *(31)*, the initial formation rate of CF was high, followed by substantial CF degradation. In the cases of $ZVI_{2L\text{-}Fh\text{-}sulfate}$ and $ZVI_{2L\text{-}Fh\text{-}phosphate}$, the increases in CT degradation rates were accompanied by fast production of CF, but no subsequent CF loss, which would be problematic if these particles were to be used in the remediation of CT. Thus, we conclude that the sulfate and phosphate anions should be avoided in the preparation of ZVI for remediation of carbon tetrachloride.

This also has implications for use of $ZVI_{2L\text{-}Fh\text{-}sulfate}$ and $ZVI_{2L\text{-}Fh\text{-}phosphate}$ in the degradation of other chlorinated groundwater contaminants, such as PCE and TCE. Hydrogenolysis of these compounds can result in intermediates that are as or more toxic

than the parent compounds *(29, 30)*. If branching ratios for compounds such as TCE are similar to those observed for CT, $ZVI_{2L\text{-}Fh\text{-}sulfate}$ and $ZVI_{2L\text{-}Fh\text{-}phosphate}$ particles would be poor choices for use for remediation as they would produce additional toxic compounds.

2.4 References

1. Li, X.-q.;Elliot, D. W. and Zhang, W.-x. *Zero-valent iron nanoparticles for abatement of environmental pollutants: materials and engineering aspects.* Critical Reviews in Solid State and Materials Sciences. **2006**, *31*, p. 111-122.

2. Elliot, D. W. and Zhang, W.-x. *Field assessment of nanoscale bimetallic particles for groundwater treatment.* Environmental Science and Technology. **2001**, *35*, p. 4922-4926.

3. Glazier, R. R.;Venkatakrishnan, F.;Gheorghiu, L.;Walata, R. and Zhang, N. W. *Nanotechnology takes root.* Civil Engineering. **2003**, *73*(5), p. 64-69.

4. Zhang, W.-x. *Nanoscale iron particles for environmental remediation: An overview.* Journal of Nanoparticle Research. **2003**, *5*, p. 1042-1047.

5. Lien, H.-L. and Zhang, W.-x. *Transformation of chlorinated methanes by nanoscale iron particles.* Journal of Environmental Engineering. **1999**, *125*, p. 1042-1047.

6. Tamara, M. L. and Butler, E. C. *Effects of iron purity and groundwater characteristics on rates and products in the degradation of carbon tetrachloride by iron metal.* Environmental Science and Technology. **2004**, *38*(1866-1876).

7. McCormick, M. L. and Adriaens, P. *Carbon tetrachloride transformation on the surface of nanoscale biogenic magnetite particles.* Environmental Science and Technology. **2004**, *38*, p. 1045-1053.

8. Bransfield, S. J.;Cwiertny, D. M.;Roberts, A. L. and Fairbrother, D. H. *Influence of copper loading and surface coverage on the reactivity of granular iron toward 1,1,1-trichloroethane.* Environmental Science and Technology. **2006**, *40*, p. 1485-1490.

9. Cwiertny, D. M.;Bransfield, S. J.;Livi, K. J. T.;Fairbrother, D. H. and Roberts, A. L. *Exploring the influence of granular iron additives on 1,1,1-trichloroethane reduction.* Environmental Science and Technology. **2006**, *40*, p. 6837-6843.

10. Kim, Y.-H. and Carraway, E. R. *Reductive dechlorination of TCE by zero valent bimetals.* Environmental Technology. **2003**, *24*, p. 69-75.

11. Cwiertny, D. M.;Bransfield, S. J. and Roberts, A. L. *Influence of the oxidizing species on the reactivity of iron-based bimetallic reductants.* Environmental Science and Technology. **2007**, *41*, p. 3734-3740.

12. Xu, Y. and Zhang, W.-x. *Subcollodial Fe/Ag particles for reduction of chlorinated benzenes.* Industrial & Engineering Chemistry Research. **2000**, *39*, p. 2238-2244.

13. Lien, H.-L. and Zhang, W.-x. *Hydroechlorination of chlorinated ethanes by nanoscale Pd/Fe bimetallic particles.* Journal of Environmental Engineering. **2005**, *131*, p. 4-10.

14. Zhang, W.-x.;Wang, C.-B. and Lien, H.-L. *Treatment of chlorinated organic contaminants with nanoscale bimetallic particles.* Catalysis Today. **1998**, *40*, p. 387-395.

15. Hassan, S. M. *Reduction of halogenated hydrocarbons in aqueous media: I. involvement of sulfur in iron catalysis.* Chemosphere. **2000**, *40*, p. 1357-1363.

16. Lipczyska-Kochany, E.;Harms, S.;Milburn, R.;Sprah, G. and Nadarajah, H. *Degradation of carbon tetrachloride in the presence of iron and sulfur containing compounds.* Chemosphere. **1994**, *29*, p. 1477-1489.

17. Devlin, J. F. and Allin, K. O. *Major anion effects on the kinetics and reactivity of granular iron in glass-encased magnet batch reactor experiments.* Environmental Science and Technology. **2005**, *39*, p. 1868-1874.

18. Liu, Y.;Phenrat, T. and Lowry, G. V. *Effect of TCE concentration and dissolved groundwater solutes on nZVI-promoted TCE dechlorination and H_2 evolution.* Environmental Science and Technology. **2007**, *41*, p. 7881-7887.

19. Johnson, T. L.;Scherer, M. M. and Tratnyek, P. G. *Kinetics of halogenated organic compound degradation by iron metal.* Environmental Science and Technology. **1996**, *30*, p. 2634-2640.

20. Schwertmann, U. and Cornell, R. M. *Iron Oxides in the Laboratory*. 2nd ed. 2000: Wiley-VCH Weinheim.

21. Erbs, J. *Insight on the reactivity of environmental iron containing nanoparticles. PhD Dissertation*. 2008, University of Minnesota.

22. Rietveld, H. M. *A profile refinement method for nuclear and magnetic structures.* Journal of Applied Crystallography. **1969**, *2*, p. 65-71.

23. Forsyth, J. B.;Johnson, C. E. and Wilkinsons, C. *The magnetic structure of vivianite, $Fe_3(PO_4)_{28}H_20$.* Journal of Physics C. Solid State Physics. **1970**, *3*, p. 1127-1139.

24. Wyckoff, R. W. G. *Crystal Structures 1*. 2nd ed. 1963, New York, NY: Interscience Publishers.

25. Okudera, H.;Kihara, K. and Matsumoto, T. *Temperature dependence of structure parameters in natural magnetite: single crystal X-ray studies from 126 to 773 K.* Acta Crystallographica. **1996**, *B 52*, p. 450-457.

26. Waychunas, G. A. *Crystal chemistry of oxides and hydroxides.* Reviews in Mineralogy. **1991**, *25*, p. 11-68.

27. Moore, P. B. *Crystal chemistry of the basic iron phosphates.* The American Mineralogist. **1970**, *55*, p. 135-169.

28. King, H. E. and Prewitt, C. T. *High-pressure and high-temperature polymorphism of iron sulfide.* Crystallographica. **1972**, *B 38*, p. 1877-1887.

29. Arnold, W. A. and Roberts, A. L. *Pathways of chlorinated ethylene and chlorinated acetylene reaction with Zn(O).* Environmental Science and Technology. **1998**, *32*(19), p. 3017-3025.

30. Bhandari, A.;Surampalli, R. Y.;Champagne, P.;Ong, S. K.;Tyagi, R. D. and Lo, I. M. C. *Remediation Technologies for Soils and Groundwater*. 2007, Reston, VA: ASCE Publications. p. 155-158.

31. Chun, C. L.;Baer, D. R.;Matson, D. W.;Amonette, J. E. and Penn, R. L. *Characterization and reactivity of iron nanoparticles prepared with added Cu, Pd, and Ni.* Environmental Science and Technology. **2010**, *44*, p. 5079-5085.

Chapter 3: Reduction of Nitroaromatic Pesticides by Fe(II)/FeOOH Systems

3.1 Introduction

Iron bearing systems are known to reduce a variety of groundwater contaminants. Surface-bound Fe(II) in particular is of major interest for its ability to quickly reduce contaminants such as chlorinated solvents and nitroaromatic compounds (NACs) *(1-6)*. Previous work has found that separately, Fe(II) and iron minerals are not effective reductants as compared to Fe(II) in the presence of iron minerals *(5, 7, 8)*.

Several factors have been found to influence the reactivity of the Fe(II)-mineral systems, including solution pH, ionic strength, and type of iron mineral present. Solution pH has been found to strongly affect adsorption of Fe(II) to the mineral surface, sufficient adsorption for contaminant transformation occuring at pH 6 and above *(5)*. The extent of sorption, in turn, has a significant effect on the reactivity of the system *(5)*. The mineral present in the system influences reactivity of surface-bound Fe(II). A study by Elsner et. al. demonstrated that Fe(II) sorbed onto the surface of iron sulfides allowed for faster reduction of hexachloroethane and 4-chloronitrobenzene when directly compared to surface area normalized rate constants for Fe(II) sorbed onto iron oxides such as hematite, magnetite, lepidocrocite, and goethite *(2)*.

Recent work has sought to better understand the reactions occurring at the Fe(II)/mineral interface. A variety of methods, including spectroscopy and atomic force microscopy, have been used to improve knowledge about electron transfer from adsorbed Fe(II) to the Fe(III) mineral surface *(8, 9)*. In particular, oxidation of Fe(II) by reductive

degradation of contaminants has been shown to occur by growth on specific faces of goethite crystals *(10, 11)*. By examining evolving reactivity of an Fe(II) – iron mineral system, insight into how natural systems evolve when minerals are continuously exposed to contaminants, can be gained. Soil particles, for example, are subject to repeated exposure to pesticides. Nitroaromatic herbicides, such as trifluralin, are repeatedly applied to and sorb to soil, where they can be degraded by Fe(II)/iron mineral systems. Understanding how the repeated exposure of iron containing soils to pesticides affects reactivity of the soil system would result in improved predictions of the fate of pesticides in the environment.

The objective of this study was to quantitatively characterize changes in goethite properties as a function of repeated exposure to Fe(II) and trifluralin and to link those changes with the evolving reactivity of the system. This was done through kinetic batch experiments in which the herbicide trifluralin was added to an Fe(II)/goethite suspension. Sequential spike experiments, in which the trifluralin concentration was restored to its initial value were also performed. All pre- and post- reaction materials were characterized using x-ray diffraction (XRD) and transmission electron microscopy (TEM). Reactions were also performed with a goethite containing sand to compare the reactivity to goethite. The goal was to compare the kinetic results with changes observed in the solid-state materials to elucidate the link between solid-state changes and changes in reaction rates.

3.2 Methods

3.2.1 Materials

All reactions were carried out in ultrapure 18MΩ•cm resistivity water (Milli-Q, Millipore). All Milli-Q water and solutions were deoxygenated by sparging with nitrogen gas. All glassware and Nalgene bottles were acid washed with 4 M HNO_3 and rinsed three times with Milli-Q water. Ferrous chloride tetrahydrate ($FeCl_2$•$4H_2O$, crystalline) was purchased from Sigma-Aldrich. Trifluralin (2,6-Dinitro-*N*,*N*-dipropyl-4-(trifluoromethyl)aniline) was purchased from Supelco. Ferrozine reagent (3-(2-pyridyl)-5,6-diphenly-1,2,3-triazine disulfonic acid disodium salt) was purchased from Acros. High purity hydrogen, nitrogen, and gas mix (95%N_2/5%H_2) gas were purchased from Airgas Inc. MOPS (3-(N-morpholino)propanesulfonic acid, sodium salt, >98% purity) was purchased from Fisher Scientific. 4-chloronitrobenze (4-Cl-NB, 99% purity) was obtained from Acros. Hexane (95+%, spectrophotometric grade) was purchased from Sigma-Aldrich. Goethite was synthesized by C. L. Chun *(11)*. Sand was obtained from Rue des Lys, Paris. The sand was yellow in color and XRD analysis determined the sand was composed of silica and goethite. Iron content in the sand was measured by inductively coupled plasma-optical emission spectroscopy (ICP-OES). The sand was 0.751 wt% iron oxide and 97 wt% silica based on ICP-OES analysis.

3.2.2 Batch Reactors

Experiments were carried out in 124 mL serum bottles in the absence of headspace. Reactors were assembled in an anaerobic glove bag (Coy Laboratory

Products, 5% H_2/95% N_2), capped with PTFE-lined septa and aluminum crimp caps and covered in aluminum foil to avoid photolysis of the trifluralin. Reactors contained 5 mg of goethite or 600 mg goethite sand (yielding approximately 5 mg of goethite) weighed directly into the bottle. Reactions were carried out in 25 mM pH 7.5 MOPS buffer. An acidified solution of 1.0 M $FeCl_2$ was added to the reactor to obtain a Fe(II) concentration of 1 mM. After addition of the $FeCl_2$ the reactor was allowed to equilibrate overnight. To initiate the reaction a methanolic stock solution of trifluralin was spiked into the reactor to achieve an initial concentration of 5 μM. The reactors were then removed from the glove bag and mixed around their longitudinal axis on a Glas-Col rotator (50 rpm) at 22 ±2 ºC. Samples were withdrawn at desired time intervals by injecting deoxygenated buffer to avoid the introduction of headspace in the reactor. Samples were extracted with hexane (1:1; v:v) on a vortex mixer for 1 minute. The extracts were analyzed by GC-MS using a Hewlett Packard G1800A GCD system. A 1 μL sample was injected by a Hewlett Packard 7673 injector autosampler onto a RTX-5 column (30 m × 0.25 mm I.D. × 0.25 μm film thickness). The oven temperature was initially held at 55 ºC for 1 minute, increased to 250 ºC at a rate of 8 ºC/minute and held for 3 minutes at 250 ºC.

After trifluralin was completely degraded, the reactor was sampled to determine the concentration of Fe(II). A modified Ferrozine method was used to quantify the Fe(II) concentration *(12)*. The reactor was then respiked with $FeCl_2$ to return the Fe(II) concentration to 1 mM. The reactor was allowed to re-equilibrate for a minimum of 1 hour before respiking the reactor with trifluralin to achieve a concentration of 5 μM. Reactors were spiked with trifluralin a total of 5 times. Samples of the goethite

suspension were taken after each reaction for TEM analysis. Each sample was centrifuged using an Eppendorf 5415 centrifuge at 2320 rcf, after which approximately three-quarters of the buffer solution was removed. Deoxygenated Milli-Q water was added to the centrifuge vial and the particles were resuspended in the water by sonication. This process was repeated a total of 3 times for each sample to prevent precipitation of buffer salt upon preparation of the TEM sample. Particles were mounted onto a TEM grid by placing a drop of the suspension on the grid. The TEM samples were prepared in the anaerobic glove bag and stored in an air-tight container until mounted onto the TEM sample holder. After all respikes were completed, particles were dried under N_2 and collected to characterize the solids by XRD.

3.2.3 4-Chloronitrobenzene Reactors

For comparison to previous work, sequential 4-Cl-NB spike batch experiments similar to the trifluralin reactions were also performed. Reactor conditions were the same as used by C. L. Chun *(11)*. Each reactor contained 0.65 g/L of goethite weighed directly into the bottle and 50 mM pH 7.0 MOPS buffer. A methanolic stock solution of 4-Cl-NB was spiked in to achieve an initial concentration of 100 μM. During the experiment, reactors were magnetically stirred in an anaerobic glove bag. Samples were withdrawn and filtered using 0.2-μm PTFE Acrodisc filters into 2.5-mL vials before being analyzed. 4-Cl-NB was analyzed by HPLC (Agilent 1100 Series) with a Zorbax C_{18} column. The mobile phase was a 70:30 mixture of acetonitrile and acetate buffer (1g/L, pH 6.9). The flow rate was 0.7 mL/min, with an injection volume of 20 μL. The absorbance at 254 nm

was monitored. Respike reactions were carried out as outlined by the trifluralin reactions.

3.2.4 Materials Characterization

XRD data were collected using a PANalytical X-Pert PRO MPD X-ray diffractometer equipped with a cobalt source and an X-Celerator detector over the range of 25-105° 2θ at a scan rate of 0.0235° per second. Diffraction patterns were compared to reference powder diffraction files (PDF) for magnetite (#19-0629), goethite (#29-0713), and quartz (46-1045).

TEM and TEM with EDS were performed using a FEI Technai T12. Particles were mounted onto 3 mm 200-mesh holey carbon-coated copper grids (Structure Probe, Inc.) in the anaerobic glove bag and stored in an air-tight container until mounted onto the TEM sample holder.

3.3 Results and Discussion

Trifluralin was degraded by the Fe(II)/goethite system within the first three hours of reaction. Kinetic data was fit using a pseudo-first order model. Plots of $\ln(C/C_0)$ versus time were linear, which indicated that the degradation of trifluralin was well described by pseudo-first order kinetics. Figure 3-1 shows a plot of the kinetic data for each spike performed. Figure 3-2 shows a plot of the pseudo-first order rate constants calculated for the sequential respikes.

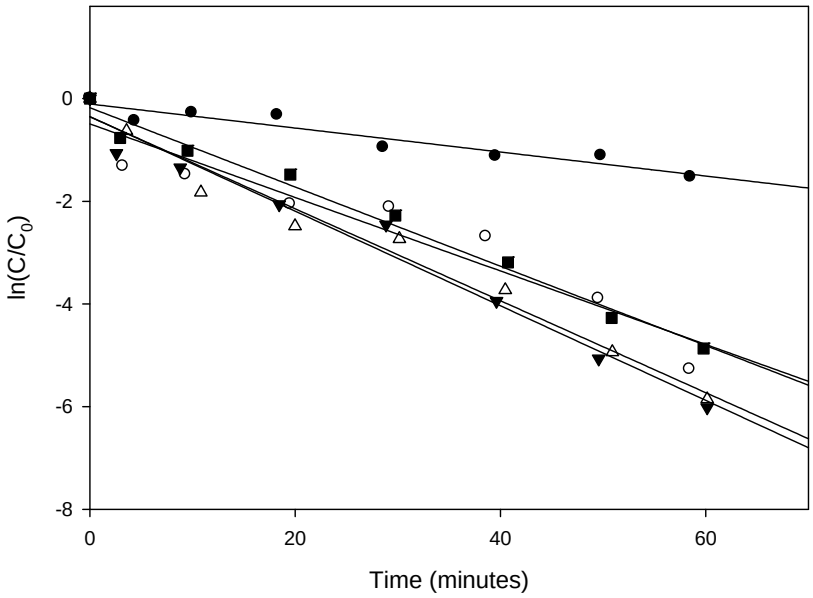

Figure 3-1. Degradation of trifluralin in sequential spike experiments with an Fe(II)/goethite suspension at pH 7.5. 1st spike (•); 2nd spike (o); 3rd spike (▼); 4th spike (Δ); 5th spike (■).

The pseudo-first order rate constant increased substantially after the first spike. Overall, the rates of reduction of trifluralin for injections #2-5 were faster than that of the original spike. Rate constants for injections #2-5 were statistically indistinguishable from each other. Approximately 10% of the Fe(II) (initial concentration 1 mmol) was used during each reaction cycle.

XRD data indicated the presence of goethite and magnetite after reaction with trifluralin after 5 reaction cycles (Figure 3-3). Magnetite was observed in TEM images after the 4th and 5th spikes, suggesting that it formed throughout the respike experiments. Previous work with these particles did not see the formation of magnetite during the

reduction of 4-Cl-NB *(11)*, suggesting that magnetite was formed as a result of reaction with trifluralin.

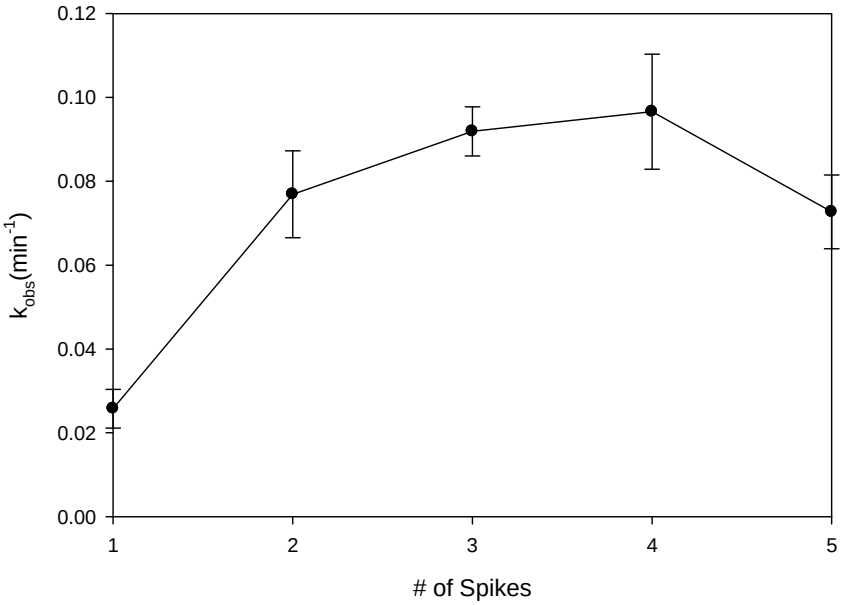

Figure 3-2. Reduction rate constants for trifluralin for five injections. Error bars are 95% confidence intervals.

The ratio of Fe(II) to goethite, however, was significantly different, in that the trifluralin experiments had a much higher ratio of Fe(II) to goethite mass compared to the 4-Cl-NB experiments. Aging experiments were performed using each system's Fe(II)/goethite loading to determine if this influenced the formation of magnetite. Contaminant blanks (i.e. batch reactors prepared with all components except for the trifluralin stock solutions) were prepared in order to test the possibility of magnetite formation due to exposure to ferrous iron. Blank reactors were placed on rotators for five days, which was the equivalent time to complete a trifluralin reaction series. XRD data for the goethite aging experiments are shown in Figure 3-4. Comparison of the XRD data

from the two goethite systems indicates an absence of magnetite in both, further supporting the idea that magnetite was formed during reaction of the trifluralin with the Fe(II)/goethite system.

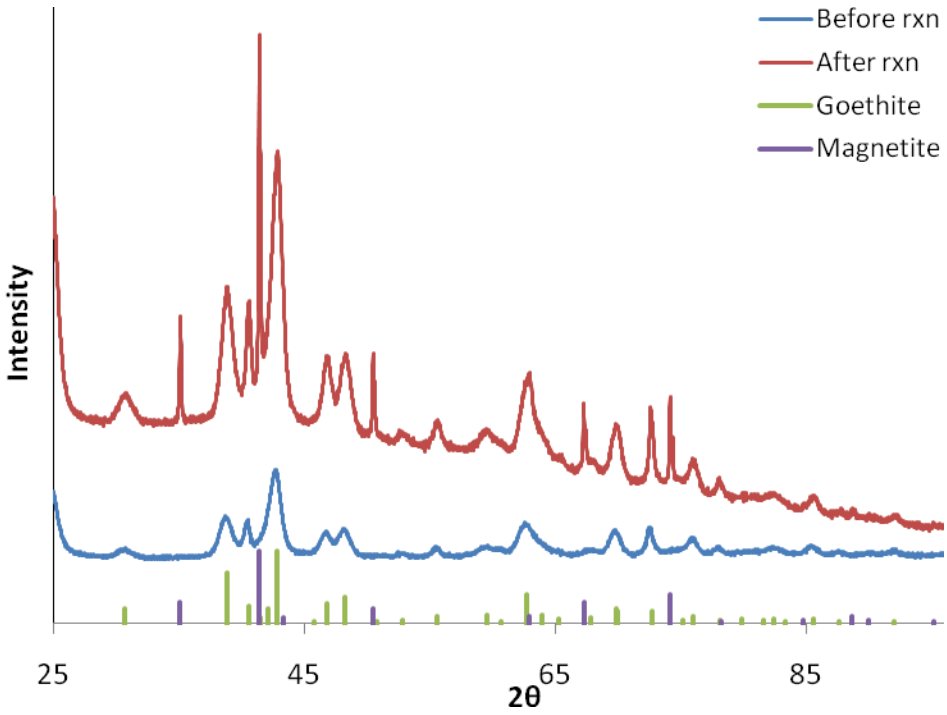

Figure 3-3. Powder XRD data for goethite before and after 5 reaction cycles with trifluralin compared with PDF reference patterns for goethite and magnetite.

TEM analysis of the goethite particles after each trifluralin spike indicated aggregation during reaction with trifluralin had occurred. Large, sea urchin-like aggregates were observed after each trifluralin spike (Figure 3-5). Individual particles, as observed before reaction, were not observed after reaction. Quantification of single crystal growth could not be performed due to the aggregation of the particles. The diameters of the aggregates were measured for each of the spikes, and average aggregate

diameters were calculated. The average diameter of the aggregates increased over the course of the injections. The density of the aggregates also appeared to increase over the course of the injections. Figure 3-6 shows a plot of the average aggregate diameters for each spike.

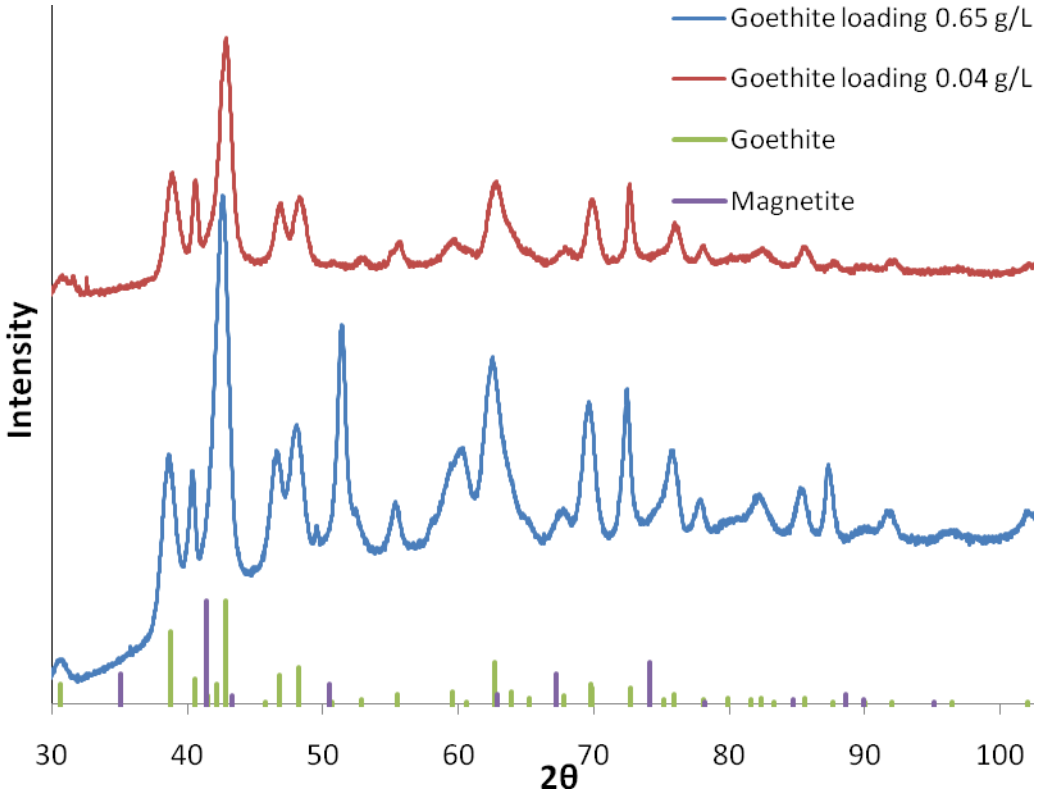

Figure 3-4. Powder XRD data for goethite aging experiments in MOPS at two different goethite loadings.

The goethite particles used during the reaction were synthesized as part of the work of C. L. Chun et. al. (*11)*. To determine if some change had occurred over that time period, experiments with 4-Cl-NB were performed again. Sequential respike experiments indicated a similar trend in the drop of reaction rates over the course of the

4-Cl-NB injections. Rate constants calculated were slightly lower, but of the same order of magnitude, as those found previously. The initial 4-Cl-NB degradation rate calculated

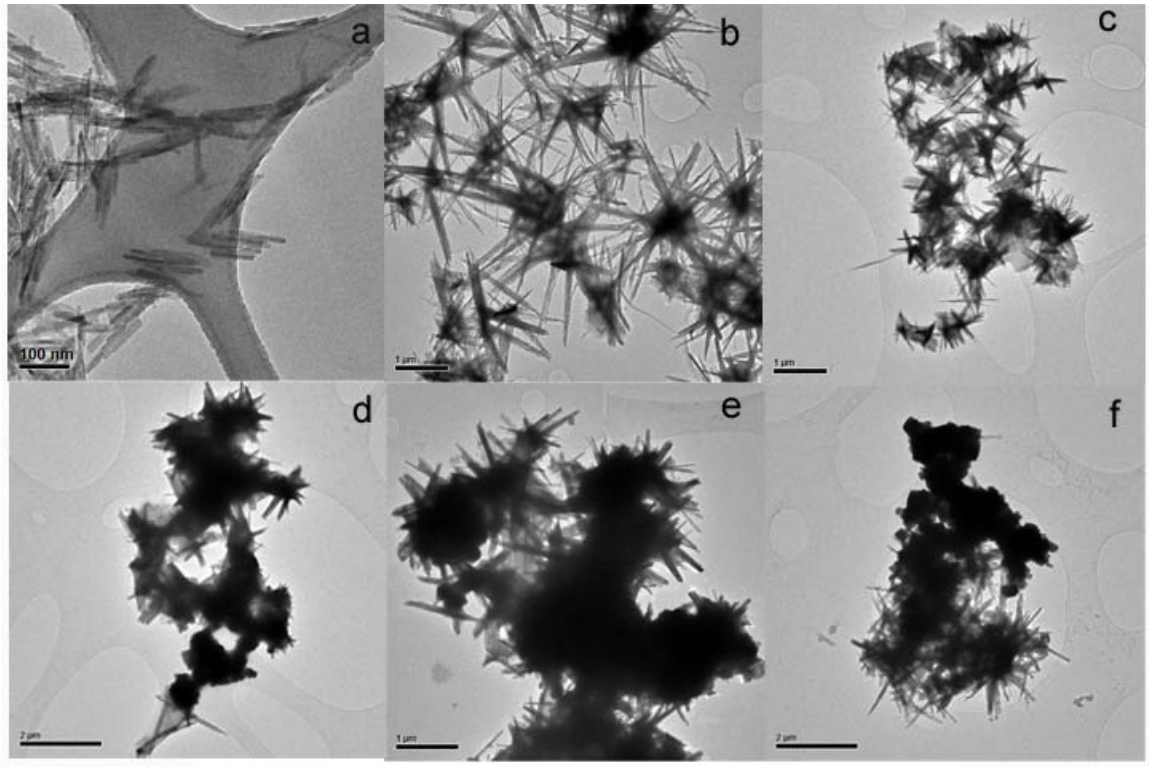

Figure 3-5. TEM images of goethite particles: a) before reaction and after each spike: b) 1st c) 2nd d) 3rd e) 4th f) 5th.

by this experiment was comparable to that of the 5th injection performed by C. L. Chun, with a value around 0.01 min^{-1}. While the rate constants were slightly lower, a large change in the particles most likely did not occur. The similar behavior observed for past and present 4-Cl-NB reactors with the goethite also suggests that the aggregation and increase in aggregate size is a product of the Fe(II)/goethite/trifluralin system.

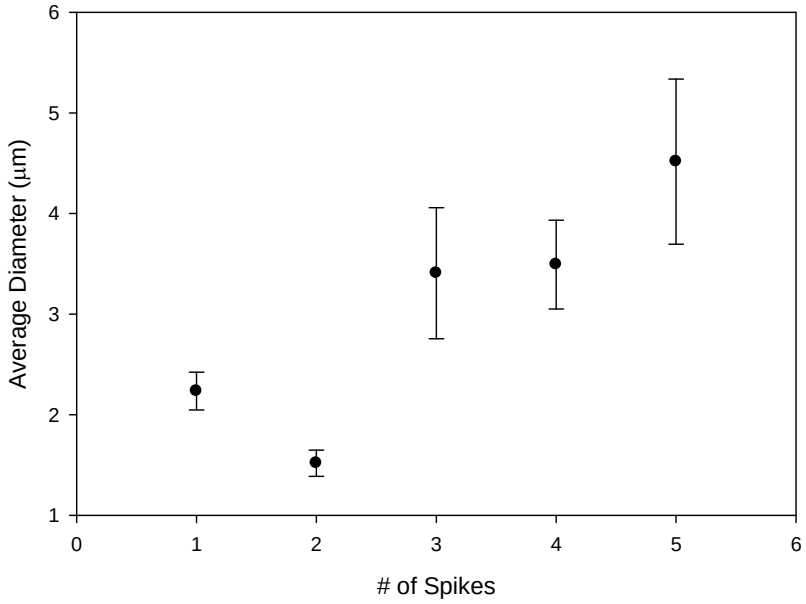

Figure 3-6. Average goethite aggregate diameters for each trifluralin spike. Error bars are 95% confidence intervals.

The increase in reactivity over the time of the Fe(II)/goethite system could be attributed to the formation of magnetite. Iron(II) with magnetite has been shown reduce nitroaromatic compounds more quickly than Fe(II) and goethite systems *(2)*. This could also account for the continuously higher reactivity of the Fe(II)/goethite systems over the course of the respikes. The increase in aggregate size could also be preserving the reactive surface of the particles, allowing for higher reaction rates after the first trifluralin spike. It also suggests that the reactions are taking place on more faces or different faces than when compared to the 4-Cl-NB, which saw particle growth in only one direction. The reduction of the trifluralin could be changing the surface of the particles along all directions, influencing the aggregation of the particles.

Reactions were also performed using trifluralin in an Fe(II)/goethite sand suspension. Trifluralin was degraded by this natural material, but at much slower rates than by the goethite nanoparticles. Rate constants for two reactors are shown in Figure 3-7. The pseudo-first order rate constants for each spike were statistically indistinguishable from one another. This implies that the reactivity of the sand is unchanged by multiple spikes of the trifluralin. Overall, the rate constants appear to decrease over the course of the respike experiments. The difference in the rate constants between the two reactors is probably due in part to the heterogeneity of natural sediments.

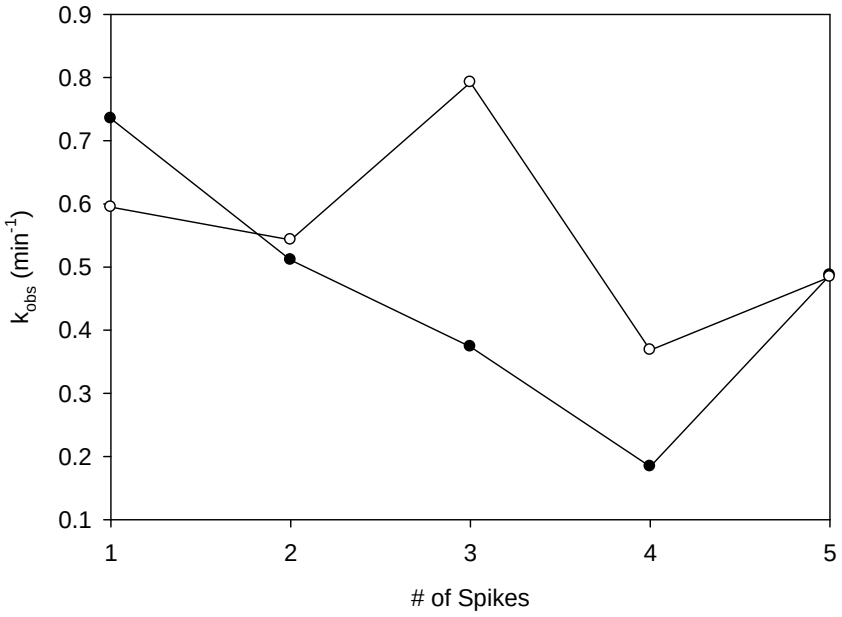

Figure 3-7. Reduction rate constants for trifluralin for five injections for reactions with Fe(II)/goethite sand suspension at pH 7.5. Data for two reactors is denoted by (●) and (○).

XRD of the sand before and after reaction (Figure 3-8) did not show any significant changes over the course of the respikes. This is likely due to the small amount

of iron present in the sand, as only 0.751 wt% was comprised of iron oxide, while 97 wt% of the sand was silica based on ICP-OES analysis of the sand. Magnetite was not detected in the sand after five reaction cycles with trifluralin. It is possible that magnetite either did not form or formed in quantities below the XRD detection limit. Comparison of the synthetic and natural goethite materials is difficult based on the data presented and would require additional work to draw more meaningful comparisons and conclusions.

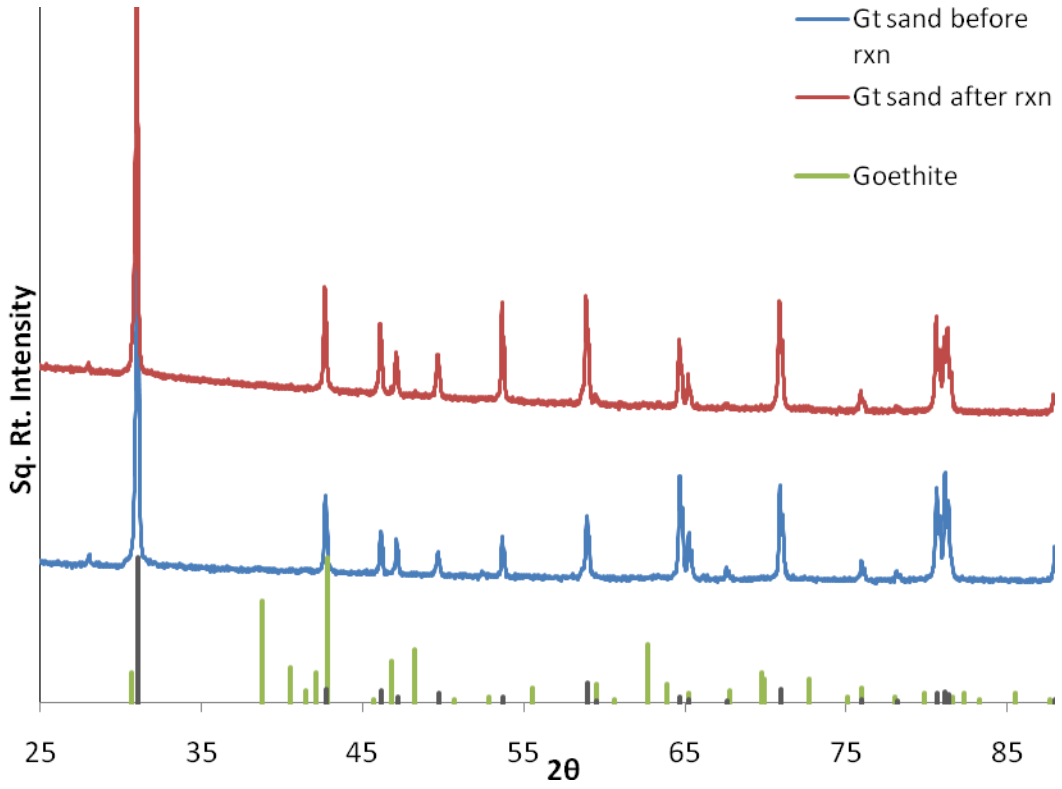

Figure 3-8. Powder XRD data for goethite sand before and after reaction with trifluralin.

3.4 References

1. Hofstetter, T. B.;Schwarzenbach, R. P. and Haderlein, S. B. *Reactivity of fe(II) species associated with clay minerals.* Environmental Science and Technology. **2003**, *37*(3), p. 519-528.

2. Elsner, M.;Schwarzenbach, R. P. and Haderlein, S. B. *Reactivity of Fe(II)-bearing minerals toward reductive transformation of organic contaminants.* Environmental Science and Technology. **2004**, *38*, p. 799-807.

3. Shultz, C. A. and Grundl, T. J. *pH dependence on reduction rate of 4-Cl-nitrobenze by Fe(II)/montmorillonite systems.* Environmental Science and Technology. **2000**, *34*, p. 3641-3648.

4. Klupinski, T. P.;Chin, Y.-P. and Traina, S. J. *Abiotic degradation of pentachloronitrobenzene by Fe(II): reactions on goethite and iron oxide nanoparticles.* Environmental Science and Technology. **2004**, *38*, p. 4353-4360.

5. Klausen, J.;Troeber, S. P.;Haderlein, S. B. and Schwarzenbach, R. P. *Reduction of substituted nitrobenzenes by Fe(II) in aqueous mineral suspensions.* Environmental Science and Technology. **1995**, *29*, p. 2396-2404.

6. Amonette, J. E.;Workman, D. J.;Kennedy, D. W.;Fruchter, J. S. and Gorby, Y. A. *Dechlorination of Carbon Tetrachloride by Fe(II) Associated with Goethite.* Environmental Science & Technology. **2000**, *34*(21), p. 4606-4613.

7. Hofstetter, T. B.;Heijman, C. G.;Haderlein, S. B.;Holliger, C. and Schwarzenbach, R. P. *Complete reduction of TNT and other (poly)nitroaromatic*

compounds under iron-reducing subsurface conditions. Environmental Science and Technology. **1999**, *33*, p. 1479-1487.

8. Williams, A. G. B. and Scherer, M. M. *Spectroscopic evidence for Fe(II)-Fe(III) electron transfer at the iron oxide - water interface.* Environmental Science and Technology. **2004**, *38*, p. 4782-4790.

9. Jun, Y.-S. and Martin, S. T. *Microscopic observation of reductive manganite dissolution under oxic conditions.* Environmental Science & Technology. **2003**, *37*, p. 2363-2370.

10. Weidler, P. G.;Hug, S. J.;Wetchc, T. P. and Hiemstra, T. *Determination of growth rates of (100) and (110) faces of synthetic goethite by scanning force microscopy.* Geochim. Cosmochim. Acta. **1998**, *62*, p. 3407-3412.

11. Chun, C. L.;Penn, R. L. and Arnold, W. A. *Kinetic and Microscopic Studies of Reductive Transformations of Organic Contaminants on Goethite.* Environmental Science and Technology. **2006**, *40*, p. 3299-3304.

12. Stookey, L. L. *Ferrozine - a new spectrophotometric reagent for iron.* Analytical Chemistry. **1970**, *42*(7), p. 779-781.

Chapter 4: Conclusions

Iron containing systems are an effective method commonly used for remediation of groundwater contaminants. Zero-valent iron is used to reduce chlorinated solvents present in groundwater. The kinetics of carbon tetrachloride reduction by ZVI materials synthesized from precursor materials containing different anions was investigated. The reactivity of ZVI synthesized from precursor materials containing chloride and nitrate were found to have no differences in reactivity as compared to each other. The presence of sulfate and phosphate was found to increase ZVI particle reactivity. Chloroform yield, however, was found to increase along with reactivity. Post-reaction products formed also varied depending on the anion present. Overall, this work suggests that ZVI particles used for remediation of carbon tetrachloride should not be synthesized from precursors containing phosphate and sulfate. Future work with ZVI particles could involve reactions containing only iron sulfide or iron phosphate in order to compare reaction rates and chloroform yields to those presented in this thesis. The particles investigated here could also be used to degrade other chlorinated compounds to compare the product yields and reaction rates.

Surface-bound Fe(II) combined with iron minerals are also effective at reducing groundwater contaminants, such as nitroaromatic pesticides. The kinetics of trifluralin degradation by Fe(II)-goethite and Fe(II)-goethite sand systems was investigated for multiple spikes of the herbicide. Trifluralin degradation rates for the Fe(II)-goethite system increased after the first spike, and then remained the same over the following spikes. Goethite particles became aggregated during reaction and the aggregates became

more dense over multiple herbicide spikes. The formation of magnetite during reaction with trifluralin was also observed. Trifluralin degradation rates for the Fe(II)-goethite sand system were smaller than those for the Fe(II)-goethite system and remained unchanged over the course of the spikes. The formation of magnetite was not observed after reaction. Overall, trifluralin was successfully degraded by synthetic and natural goethite. Further conclusions are difficult to draw without performing additional work. Future work could include experiments that examine the effect of different goethite loadings on rate constants and particle morphology. The experiments performed in this thesis could also be repeated with a series of reactors such that a reactor could be broken down for a solids analysis after each respike. This would provide insight on magnetite formation and goethite aggregation over the course of the respike experiments. Conducting additional trifluralin degradation experiments using the goethite sand would also allow better conclusions about the reaction rates after each respike.

Bibliography

Amonette, J. E.;Workman, D. J.;Kennedy, D. W.;Fruchter, J. S. and Gorby, Y. A. *Dechlorination of Carbon Tetrachloride by Fe(II) Associated with Goethite.* Environmental Science & Technology. **2000**, *34*(21), p. 4606-4613.

Arnold, W. A. and Roberts, A. L. *Pathways of chlorinated ethylene and chlorinated acetylene reaction with Zn(O).* Environmental Science and Technology. **1998**, *32*(19), p. 3017-3025.

Barcelona, M. J. *Contamination of Ground water: Prevention, Assessment, Restoration*. 184 ed. Pollution Technology Review. 1990: William Andrew, Incorporated. p. 228.Air Toxics Website: Chloroform. http://www.epa.gov/ttn/atw/hlthef/chlorofo.html (July, 2010).

Bhandari, A.;Surampalli, R. Y.;Champagne, P.;Ong, S. K.;Tyagi, R. D. and Lo, I. M. C. *Remediation Technologies for Soils and Groundwater*. 2007, Reston, VA: ASCE Publications. p. 155-158.

Bicki, T. J. *Pesticides and Groundwater: Pesticides as Potential Pollutants*; University of Illinois at Urbana-Champaign College of Agricultural, Consumer and Environmental Sciences: 1989; p. 3-9.

Bransfield, S. J.;Cwiertny, D. M.;Roberts, A. L. and Fairbrother, D. H. *Influence of copper loading and surface coverage on the reactivity of granular iron toward 1,1,1-trichloroethane.* Environmental Science and Technology. **2006**, *40*, p. 1485-1490.

California EPA. *In situ groundwater remediation at sites with volatile organic compounds, nitrogen compounds, perchlorate, pesticides, semi-volatile compounds and/or petroleum hydrocarbons*; State Water Resources Control Board, California EPA: CA, 2007; p. 1-8.

Charlet, L.;Silvester, E. and Lifer, E. *N-compound reduction and actinide immobilisation in surficial fluids by Fe(II): the surface* $Fe^{III}OFe^{II}OOH^{o}$ *species, as major reductant.* Chemical Geology. **1998**, *151*, p. 85-93.

Chun, C. L.;Penn, R. L. and Arnold, W. A. *Kinetic and Microscopic Studies of Reductive Transformations of Organic Contaminants on Goethite.* Environmental Science and Technology. **2006**, *40*, p. 3299-3304.

Chun, C. L.;Baer, D. R.;Matson, D. W.;Amonette, J. E. and Penn, R. L. *Characterization and reactivity of iron nanoparticles prepared with added Cu, Pd, and Ni.* Environmental Science and Technology. **2010**, *44*, p. 5079-5085.

Colborn, T. and Short, P. *Pesticide use in the U.S and policy implications: A focus on herbicides.* Toxicology and Industrial Health. **1999**, *15*, p. 241-276.

Cwiertny, D. M.;Bransfield, S. J.;Livi, K. J. T.;Fairbrother, D. H. and Roberts, A. L. *Exploring the influence of granular iron additives on 1,1,1-trichloroethane reduction.* Environmental Science and Technology. **2006**, *40*, p. 6837-6843.

Cwiertny, D. M.;Bransfield, S. J. and Roberts, A. L. *Influence of the oxidizing species on the reactivity of iron-based bimetallic reductants.* Environmental Science and Technology. **2007**, *41*, p. 3734-3740.

Delleur, J. W. *The Handbook of Groundwater Engineering, 2nd Edition*. 2006, Boca Raton, FL: CRC Press. p. 36-30 - 36-33.

Devlin, J. F.;Klausen, J. and Schwarzenbach, R. P. *Kinetics of nitroaromatic reduction on granular iron in recirculating batch experiments.* Environmental Science and Technology. **1998**, *32*, p. 1941-1947.

Devlin, J. F. and Allin, K. O. *Major anion effects on the kinetics and reactivity of granular iron in glass-encased magnet batch reactor experiments.* Environmental Science and Technology. **2005**, *39*, p. 1868-1874.

Elliot, D. W. and Zhang, W.-x. *Field assessment of nanoscale bimetallic particles for groundwater treatment.* Environmental Science and Technology. **2001**, *35*, p. 4922-4926.

Elsner, M.;Schwarzenbach, R. P. and Haderlein, S. B. *Reactivity of Fe(II)-bearing minerals toward reductive transformation of organic contaminants.* Environmental Science and Technology. **2004**, *38*, p. 799-807.

EPA. In *Proceedings of the Symposium on Natural Attenuation of Chlorinated Organics*, Dallas, Texas, 1996; EPA, Office of Research and Development, U.S. EPA: Dallas, Texas, 1996; p. 7-11.

EPA. *In Situ Thermal Treatment of Chlorinated Solvents: Fundamentals and Field Applications*. EPA 542-R-04-010. 2004, Washington, D.C.: U.S. EPA Office of Solid Waste and Emergency Response. p. 7-12.

Erbs, J. *Insight on the reactivity of environmental iron containing nanoparticles. PhD Dissertation*. 2008, University of Minnesota.

Farrell, J.;Kason, M.;Melitas, N. and Li, T. *Investigation of the long-term performance of zero-valent iron for reductive dechlorination of trichloroethylene.* Environmental

Science and Technology. **2000**, *34*(3), p. 512-521.

Forsyth, J. B.;Johnson, C. E. and Wilkinsons, C. *The magnetic structure of vivianite, $Fe_3(PO_4)_{28}H_20$.* Journal of Physics C. Solid State Physics. **1970**, *3*, p. 1127-1139.

Gasnier, C.;Dumont, C.;Benachour, N.;Clair, E.;Chagnon, M.-C. and Seralini, G.-E. *Glyphosate-based herbicides are toxic and endocrine disruptors in human cell lines.* Toxicology. **2009**, *262*(3), p. 184-191.

Gilliom, R. J. and Hamilton, P. A. *Pesticides in the Nation's Streams and Ground Water: 1992-2001 A Summary*; USGS: Sacramento, CA, 2006; p. 1-6.

Glazier, R. R.;Venkatakrishnan, F.;Gheorghiu, L.;Walata, R. and Zhang, N. W. *Nanotechnology takes root.* Civil Engineering. **2003**, *73*(5), p. 64-69.

Hassan, S. M. *Reduction of halogenated hydrocarbons in aqueous media: I. involvement of sulfur in iron catalysis.* Chemosphere. **2000**, *40*, p. 1357-1363.

He, Y. T. and Traina, S. J. *Transformation of magnetite to goethite under alkaline pH conditions.* Clay Minerals. **2007**, *42*, p. 13-19.

Hofstetter, T. B.;Heijman, C. G.;Haderlein, S. B.;Holliger, C. and Schwarzenbach, R. P. *Complete reduction of TNT and other (poly)nitroaromatic compounds under iron-reducing subsurface conditions.* Environmental Science and Technology. **1999**, *33*, p. 1479-1487.

Hofstetter, T. B.;Schwarzenbach, R. P. and Haderlein, S. B. *Reactivity of fe(II) species associated with clay minerals.* Environmental Science and Technology. **2003**, *37*(3), p. 519-528.

Jeffers, P. M.;Ward, L. M.;Woytowitch, L. M. and Wolfe, N. L. *Homogeneous hydrolysis rate constants for selected chlorinated methanes, ethanes, ethenes, and propanes.* Environmental Science and Technology. **1989**, *23*(8), p. 965-969.

Johnson, T. L.;Scherer, M. M. and Tratnyek, P. G. *Kinetics of halogenated organic compound degradation by iron metal.* Environmental Science and Technology. **1996**, *30*, p. 2634-2640.

Jun, Y.-S. and Martin, S. T. *Microscopic observation of reductive manganite dissolution under oxic conditions.* Environmental Science & Technology. **2003**, *37*, p. 2363-2370.

Keily, T.;Donaldson, D. and Grube, A. *Pesticides Industry Sales and Usage: 2000 and 2001 Market Estimates*; U.S. EPA Office of Prevention, Pesticides, and Toxic Substances: Washington, D.C., 2004; p. 16-31.

Keum, Y.-S. and Li, Q. X. *Reduction of nitroaromatic pesticides with zero-valent iron.* Chemosphere. **2004**, *54*, p. 255-263.

Kim, Y.-H. and Carraway, E. R. *Reductive dechlorination of TCE by zero valent bimetals.* Environmental Technology. **2003**, *24*, p. 69-75.

King, H. E. and Prewitt, C. T. *High-pressure and high-temperature polymorphism of iron sulfide.* Crystallographica. **1972**, *B 38*, p. 1877-1887.

Klausen, J.;Troeber, S. P.;Haderlein, S. B. and Schwarzenbach, R. P. *Reduction of substituted nitrobenzenes by Fe(II) in aqueous mineral suspensions.* Environmental Science and Technology. **1995**, *29*, p. 2396-2404.

Klupinski, T. P.;Chin, Y.-P. and Traina, S. J. *Abiotic degradation of pentachloronitrobenzene by Fe(II): reactions on goethite and iron oxide nanoparticles.* Environmental Science and Technology. **2004**, *38*, p. 4353-4360.

Lai, K. C.-K. and Lo, I. M.-C. In *Field monitoring of the performance of a PRB at the Vapokon site, Denmark.*, Permeable Reactive Barriers (PBRs) Action Team Meeting, Niagara Falls, New York, October 15-16, 2003; Niagara Falls, New York, 2003.

Lai, K. C. K.;Lo, I. M. C. and Kjeldsen, P. In *Permeable Reactive Barriers*, 1st International Symposium on Permeable Reactive Barriers, Belfast, Northern Ireland, March 14-16, 2004; Genevieve A. Boshoff and Brian D. Bone, International Association of Hdyrological Sciences: Belfast, Northern Ireland, 2004; p. 12-22.

Lee, C. C. and Lin, S. D. *Water and Wastewater Calculations Manual*. 2nd ed. 2007: McGraw-Hill Professional. p. 211-214.

Li, X.-q.;Elliot, D. W. and Zhang, W.-x. *Zero-valent iron nanoparticles for abatement of environmental pollutants: materials and engineering aspects.* Critical Reviews in Solid State and Materials Sciences. **2006**, *31*, p. 111-122.

Liang, L.;Korte, N.;Gu, B.;Puls, R. and Reeter, C. *Geochemical and microbial reactions affecting the long-term performance of in situ "iron barriers".* Advances in Environmental Research. **2000**, *4*(4), p. 273-286.

Lien, H.-L. and Zhang, W.-x. *Transformation of chlorinated methanes by nanoscale iron particles.* Journal of Environmental Engineering. **1999**, *125*, p. 1042-1047.

Lien, H.-L. and Zhang, W.-x. *Hydroechlorination of chlorinated ethanes by nanoscale Pd/Fe bimetallic particles.* Journal of Environmental Engineering. **2005**, *131*, p. 4-10.

Lipczyska-Kochany, E.;Harms, S.;Milburn, R.;Sprah, G. and Nadarajah, H. *Degradation of carbon tetrachloride in the presence of iron and sulfur containing compounds.* Chemosphere. **1994**, *29*, p. 1477-1489.

Liu, Y.;Majetich, S. A.;Tilton, R. D.;Sholl, D. S. and Lowry, G. V. *TCE dechlorination rates, pathways, and efficiency of nanoscale iron particles with different properties.* Environmental Science and Technology. **2005**, *39*(5), p. 1338-1345.

Liu, Y.;Phenrat, T. and Lowry, G. V. *Effect of TCE concentration and dissolved groundwater solutes on nZVI-promoted TCE dechlorination and H_2 evolution.* Environmental Science and Technology. **2007**, *41*, p. 7881-7887.

Matheson, L. J. and Tratnyek, P. G. *Reductive dehalogenation of chlorinated methanes by iron metal.* Environmental Science and Technology. **1994**, *28*, p. 2045-2053.

Matthews, G. A. *Pesticides: Health, Safety, and the Environment*. 2006, Ames, IA: Wiley-Blackwell. p. 42-43.

McCarty, P. L. In *Groundwater quality: natural and enhanced restoration of groundwater*, Groundwater Quality 2001, Sheffield, UK, 2001; Sascha E. Oswald Steven F. Thornton, International Association of Hydrological Sciences: Sheffield, UK, 2001; p. 319-325.

McCormick, M. L. and Adriaens, P. *Carbon tetrachloride transformation on the surface of nanoscale biogenic magnetite particles.* Environmental Science and Technology. **2004**, *38*, p. 1045-1053.

Moore, P. B. *Crystal chemistry of the basic iron phosphates.* The American Mineralogist. **1970**, *55*, p. 135-169.

National Research Council Committee of Innovative Remediation Technologies, ed. *Innovations in Ground Water and Soil Cleanup: From Concept to Commercialization*. 1997, National Academies Press: Washington D.C. 113-120.

Nurmi, J. T.;Tratnyek, P. G.;Sarathy, V.;Linehan, J. C.;Matson, D. W.;Penn, R. L. and Driessen, M. D. *Characterization and properties of metallic iron nanoparticles: Spectroscopy, electrochemistry, and kinetics.* Environmental Science and Technology. **2005**, *39*, p. 1221-1230.

Okudera, H.;Kihara, K. and Matsumoto, T. *Temperature dependence of structure parameters in natural magnetite: single crystal X-ray studies from 126 to 773 K.* Acta Crystallographica. **1996**, *B 52*, p. 450-457.

Pesticides: Health and Safety: Human Health Issues. http://www.epa.gov/pesticides/health/human.htm (July, 2010).

Rietveld, H. M. *A profile refinement method for nuclear and magnetic structures.* Journal of Applied Crystallography. **1969**, *2*, p. 65-71.

Roberts, A. L.;Totten, L. A.;Arnold, W. A.;Burris, D. R. and Campbell, T. J. *Reductive elimination of chlorinated ethylenes by zero-valent metals.* Environmental Science and Technology. **1996**, *30*(8), p. 2654-2659.

Roberts, D. J. *Use of Landfarming to Remediate Soil Contaminated by Pesticides*. 1995, Springfield, IL: DIANE Publishing. p. 40-41.

Rugge, K.;Hofstetter, T. B.;Haderlein, S. B.;Bjerg, P. L.;Knudsen, S.;Zraunig, C.;Mosbek, H. and Christensen, T. H. *Characterization of predominant reductants in an anaerobic leachate-contaminated aquifer by nitroaromatic probe compounds.* Environmental Science & Technology. **1998**, *32*(1), p. 23-31.

Schwertmann, U. and Cornell, R. M. *Iron Oxides in the Laboratory*. 2nd ed. 2000: Wiley-VCH Weinheim.

Shultz, C. A. and Grundl, T. J. *pH dependence on reduction rate of 4-Cl-nitrobenze by Fe(II)/montmorillonite systems.* Environmental Science and Technology. **2000**, *34*, p. 3641-3648.

Stookey, L. L. *Ferrozine - a new spectrophotometric reagent for iron.* Analytical Chemistry. **1970**, *42*(7), p. 779-781.

Tamara, M. L. and Butler, E. C. *Effects of iron purity and groundwater characteristics on rates and products in the degradation of carbon tetrachloride by iron metal.* Environmental Science and Technology. **2004**, *38*(1866-1876).

USGS Groundwater use in the United States. http://ga.water.usgs.gov/edu/wugw.html (July, 2010).

Vikesland, P. J.;Heathcock, A. M.;Rebodos, R. L. and Makus, K. E. *Particle size and aggregation effects on magnetite reactivity toward carbon tetrachloride.* Environmental Science and Technology. **2007**, *41*, p. 5277-5283.

Wang, C.-B. and Zhang, W.-X. *Synthesizing nanoscale iron particles for rapid and complete dechlorination of TCE and PCBs.* Environmental Science and Technology. **1997**, *31*, p. 2154-2156.

Waychunas, G. A. *Crystal chemistry of oxides and hydroxides.* Reviews in Mineralogy. **1991**, *25*, p. 11-68.

Weber, E. J. *Iron-Mediated Reductive Transformations: Investigation of Reaction Mechanism.* Environmental Science and Technology. **1996**, *30*, p. 716-719.

Weidler, P. G.;Hug, S. J.;Wetchc, T. P. and Hiemstra, T. *Determination of growth rates of (100) and (110) faces of synthetic goethite by scanning force microscopy.* Geochim. Cosmochim. Acta. **1998**, *62*, p. 3407-3412.

Wetzel, R. G. *Limnology*. 2nd ed. 1983, Philadelphia: Saunders College Publishing. p. 261-263.

Williams, A. G. B. and Scherer, M. M. *Spectroscopic evidence for Fe(II)-Fe(III) electron transfer at the iron oxide - water interface.* Environmental Science and Technology. **2004**, *38*, p. 4782-4790.

Wyckoff, R. W. G. *Crystal Structures 1*. 2nd ed. 1963, New York, NY: Interscience Publishers.

Xu, Y. and Zhang, W.-x. *Subcollodial Fe/Ag particles for reduction of chlorinated benzenes.* Industrial & Engineering Chemistry Research. **2000**, *39*, p. 2238-2244.

Zhang, W.-x.;Wang, C.-B. and Lien, H.-L. *Treatment of chlorinated organic contaminants with nanoscale bimetallic particles.* Catalysis Today. **1998**, *40*, p. 387-395.

Zhang, W.-x. *Nanoscale iron particles for environmental remediation: An overview.* Journal of Nanoparticle Research. **2003**, *5*, p. 1042-1047.